Direct Observations of Scavenging Reactions of the Prehydrated Electron and $^{\bullet}$OH Radicals by Femtosecond Time-Resolved Laser Spectroscopy

by

Yuhan Ma

A thesis
presented to the University of Waterloo
in fulfillment of the
thesis requirement for the degree of
Master of Science
in
Physics

Waterloo, Ontario, Canada, 2011

I hereby declare that I am the sole author of this thesis. This is a true copy of the thesis, including any required final revisions, as accepted by my examiners.

I understand that my thesis may be made electronically available to the public.

Abstract

Radiotherapy is the major curative therapy for carcinogesis. Identifying the effective species that induce DNA damage under ionizing radiation holds the key to improve and advance radiotherapy. In a cellular environment, most of the radiation energy is absorbed by water in the cell. Traditionally, the major radicals resulting from the radiolysis of water are thought to be the hydroxyl radical ($^{\bullet}$OH) and the hydrated electron, whereas the ($^{\bullet}$OH) radical is considered as the major contributor to radiation-induced DNA damage. With the birth of femtosecond time-resolved laser spectroscopy, the precursor to the hydrated electron, the so-called prehydrated electron, has been directly observed. The prehydrated electrons are the excited states of the well-known hydrated electron in nature. Very recently, it was pointed out that the prehydrated electron is a reactive species capable of causing lethal DNA double strand breaks. Thus the reductive DNA damage is proposed as a new molecular pathway for radiation-induced DNA damage. Therefore, the reaction dynamics of the prehydrated electron is of great interest to unravel the exact mechanism of radiation-induced DNA damage.

In order to study the action of the prehydrated electron (e_{pre}^{-}) in biologically relevant reactions, additional compounds need to be applied to regulate the prehydrated electrons. Such compounds are electron scavengers. In this thesis, the ultrafast electron transfer reaction of e_{pre}^{-} with an electron scavenger potassium nitrate was first investigated using our state-of-the-art femtosecond time-resolved pump-probe laser spectroscopy (fs-TRLS). Quantitative scavenging efficiency is successfully obtained by measuring the reaction rate constant, which is determined to be $k_{pre} = (0.75 \pm 0.5) \times 10^{13}$ M^{-1}s^{-1}. This value is two-orders larger than the reaction rate constant of e_{hyd}^{-} with potassium nitrate $k = 9.7 \times 10^{9}$ M^{-1}s^{-1}, confirming the high reactivity of e_{pre}^{-}.

Moreover, to comparing effectiveness of the reductive DNA damage induced by the prehydrated electron to the oxidative DNA damage induced by OH radicals, OH radical scavengers are used to quench OH radicals, leaving the prehydrated electron as the only active species. However, no studies have ever investigated the reactions between OH radical

scavengers and the prehydrated electron. Here we performed the first quantitative study on the scavenging reactions of e_{pre}^- with the well-known OH radical scavengers, isopropanol and dimethyl sulfoxide (DMSO). We present the first evidence of such scavenging reactions and determine the reaction rate constants, which are measured to be $k = 3.3 \pm 0.5 \times 10^{11}$ $M^{-1}s^{-1}$ and $8.7 \pm 0.5 \times 10^{11}$ $M^{-1}s^{-1}$ for isopropanol and DMSO in PBS buffer, respectively. These values are much higher than the reaction rate constants of isopropanol with ${}^{\bullet}OH$ radicals and DMSO with ${}^{\bullet}OH$ radicals ($k_{isopropanol+OH} = 2 \times 10^9$ $M^{-1}s^{-1}$ and $k_{DMSO+OH} = 7 \times 10^9$ $M^{-1}s^{-1}$).

Furthermore, the OH radical is an important species produced from radiolysis of water. Knowing its reaction dynamics and kinetics can facilitate the comparison between the oxidative DNA damage induced by OH radicals and the reductive DNA damage by prehydrated electrons. By using an OH radical scavenger KSCN, we are able to directly observe the reaction dynamics of the OH radical. In addition, knowing the relative yield ratio of OH radicals and the e_{pre}^- ($r = [{}^{\bullet}OH]/[e_{pre}^-]$) is necessary for the comparison of the effectiveness of e_{pre}^- and OH radicals at inducing DNA damage. In our study, a quantitative analysis of the relative yield ratio r using an OH radical scavenger KSCN was obtained. The relative yield ratio is determined to be $r = [{}^{\bullet}OH]/[e_{pre}^-] = 2.8 \pm 0.4$. Incorporating this value into our recent studies on reductive DNA damage, we find that in terms of single-strand breaks and double-strand breaks yields per radical, an e_{pre}^- is nearly three times as effective as an ${}^{\bullet}OH$ at inducing DNA damage under irradiation. Overall, the results obtained from this thesis provide important information for future studies of e_{pre}^- action in biologically relevant reactions.

Acknowledgements

I would like to thank my supervisor Dr. Qing-Bin Lu for his helpful guidance, generous support and encouragement throughout my undergraduate and graduate studies. I also would like to thank all my group members at our femtobiology and femtomedicine lab, for their friendship and support. Lastly, I would like to thank Ting Luo for her valuable discussions.

My gratitude also goes to my parents for being there for me, and all my friends, for the happiness they have brought to my life.

To My Parents

Table of Contents

List of Figures

List of Tables

Chapter 1

Introduction

1.1 Cancer and cancer therapies

Carcinogenesis is one of the most malicious human diseases. It is an abnormal growth of cells that arises from the changes in gene expressions, leading to the imbalance between cell proliferation and cell death. Ultimately, the abnormal cancerous cells can invade tissues, causing serious morbidity, and if not treated, leading to the death of the host. Though many diseases become curable with the advent of science, cancer still remains a life-threatening disease. Moreover, the number of cancer patients is increasing each year with an estimated number of 20 millions in next 20 years worldwide [1]. Therefore, more effective cancer therapies are highly desirable for the benefit of all human beings. Cancer research aims to understand cancer at the molecular level to develop more effective cancer therapies to control cancer. Three major treatments for cancer are: surgery, chemotherapy and radiotherapy.

1.1.1 Surgery

Surgery intends to remove the tumour tissues from a patient for diagnosis or treatment purposes. For diagnosis, only a small piece of tumour is removed. This procedure is called a biopsy. Following diagnosis, surgery can be performed to stage, to treat or debulk tumours. Debulking is a procedure used to remove tumours as much as possible to increase the effectiveness of other therapies when it is impossible to remove the entire tumour without harming healthy organs. The surgeon usually removes the tumour and some surrounding healthy tissues (know as a "clear margin") to ensure that all of the cancer is removed. If the cancer is diagnosed at an early stage, surgery alone may prevent cancer from developing. Otherwise, surgery is often combined with chemotherapy or radiotherapy. Though surgery is the most straightforward treatment for cancer, it can cause several side effects in cancer patients such as organ dysfunction, lymphedema and reoccurrence of cancer, etc.

1.1.2 Chemotherapy

Chemotherapeutic agents target tumour cells in order to prevent the cells from multiplying, proliferating and killing patients. It is based on the principle that rapidly growing tumours are more susceptible to cytotoxic agents than normal tissues. The commonly used chemotherapeutic agents can be catalogued into three major types: cytotoxic agents, anti-hormonal drugs and targeted drugs. Cytotoxic drugs are the most traditional chemotherapeutic agents. They mainly target DNA molecules to either inhibit cell division or DNA synthesis. Cytotoxic drugs remain the largest group of chemotherapeutic drugs and they have the most general applications for various types of cancer. More specifically, for breast and prostate tumours subject to hormonal regulations, anti-hormonal drugs are primary curative agents. For example, breast tumour cell growth is closely related to the estrogen level in cancer patients. By attacking estrogen receptors, anti-hormonal drugs can inhibit breast tumour cell growth. Similarly, androgen receptors are targets for anti-hormonal drugs in the treatments of prostate cancer [2]. Moreover, the characterization of "the hallmarks of cancer" leads to the understanding of malignant cell growth at the molecular level[3]. Another newly developed group of chemo drugs inhibit the macromolecular targets that are essential to tumours but not present in normal organs and tissues. These drugs are termed targeted drugs, and they were introduced during 1997-2004, followed by the approval of monoclonal antibody Rituximab (RITUXAN^{TM}) by the FDA for the treatment of Non-Hodgkin's lymphoma [2]. The targeted drugs are designed to have better selectivity than traditional cytotoxic drugs. However, the targeted drugs are still under development and not yet widely available.

Many of the strong side effects caused by cytotoxic drugs arise from the effects of these drugs on normal cells. The side effects of chemotherapy include uncomfortable feelings in patients following drug uptakes, serious compromises of most organs of the body, drug resistance in the tumour cells and therapy limiting effects of bone marrow toxicity.

1.1.3 Radiotherapy

Radiotherapy deposits radiation energy into a tumour tissue to kill cancer cells through ionization or excitation of the biological materials. Though normal tissue cells may also be affected by radiation, they have better cell repair mechanism to recover from the radiation damage. Moreover, the major delivery of radiotherapy can be carefully controlled and localized within tumour tissues with the aid of various software and hardware. Cancer patients treated with radiotherapy may experience side effects such as tiredness, skin soreness, loss of red blood cells (anemia) and nausea. Moreover, hypoxic regions in solid tumour can reduce radiotherapy efficiency.

The most commonly used radiation sources are the x-rays or γ-rays, both of which are electromagnetic radiations. Radiation interacts with biological materials through either an ionization or excitation process. If sufficient radiation energy was deposited to eject one or more orbital electrons from the atoms or molecules with which it interacts, the atom is ionized. Whenever the energy of a photon or particle exceeds the ionization potential of a molecule, a collision with the molecule can lead to ionization. On the other hand, if the radiation energy is below the ionization of a molecule, radiation energy is transferred without any ejections of electrons. Such processes are termed as excitations. Excitation brings an electron to a higher energy level without actually displacing it. In general, for biological materials, photons or particles with energies above 10 eV are considered as ionizing radiations whereas excitations occur under 10 eV. The dose of radiation to biological material is defined in terms of the amount of energy absorbed per unit mass. 1 Gy is equivalent to 1 J/kg.

Radiation energy deposition in biological system create both free electrons and excited electrons. These electrons will further interact with biological materials to ionize or excite biological molecules. Radiotherapy mainly attacks the genetic material deoxyribonucleic acid, commonly known as DNA. Radiation-induced DNA damage is a precursor of genomic instability, mutations and cell death. Detailed pathways of radiation-induced DNA damage will be introduced later in this chapter.

Another type of radiation source is the particulate radiation source including electrons, protons, α-particles, neutrons, negative π-mesons, and heavy charged ions. These radiation sources produce particles that interact with biological materials in similar ways. Considering the fact that these sources are much less commonly used, they are beyond the scope of this thesis.

1.1.4 Other therapies

In addition to the three major therapies above, there are other relatively new therapies in use for cancer treatments. These therapies include photodynamic therapy, gene therapy, etc.

Photodynamic therapy (PDT) is a relatively new method currently approved as treatments for some forms of cancer including skin cancer, cervical cancer, lung cancer, superficial gastric cancer, superficial bladder cancer., etc. [4,5]. PDT combines the effect of visible light with a photosensitizing compound and oxygen. The photosensitizer (PS) is specifically accumulated in the tumour tissues, which is then selectively exposed to a long-wavelength visible light ($\lambda \geq 600$ nm) so that the PS within the tissue is excited upon illumination. The excitation energy is transferred to the oxygen to give rise to damaging singlet oxygen and other reactive oxygen species (ROS) [5,6]. These reactive oxygen species are cytotoxic photoproducts, which initiate a chain of biochemical events that induce damage and the death of tumour cells. The use of PDT as a cancer therapy is attractive because of its specificity and selectivity. Although PDT is a promising cancer therapy, the selection of PS is limited by a number of factors: PS must have good stability, must be retained by tumour tissues, must have minimal toxicity in the absence of light, must become cytotoxic upon light radiation and must absorb light with longer wavelength. Because the longer the wavelength, the deeper the light penetration to the tumour tissues [5,7,8]. Therefore, PDT is limited to treat tumour tissues that are accessible by light penetration or optical fiber delivery. Currently, seeking suitable photosensitizers to improve PDT application remains the main task of PDT research.

Gene therapy for cancer is another developing cancer therapy, which is based on the simple idea to introduce the right gene in cells so that the products of the gene can cure or slow down the progression of cancer. However, the realization of gene therapy is not as simple at

all. The obstacles of gene therapy include finding suitable vectors to transduce genes into the host cells and the immune response of the host can cease gene delivery process [9]. Hence, not until difficulties are solved, can gene therapy be applied widely to benefit cancer patients.

1.2 Radiation-Induced DNA Damage

Among all three major treatments for cancer mentioned, radiotherapy is the most widely used approach. Approximately 50-70% of all cancer patients have been treated with radiotherapy [10]. The genetic material deoxyribonucleic acid, commonly known as DNA, is the principal target for the biological effects of ionizing radiation. Radiation-induced DNA damage can induce genomic instability, mutations and cell death. Therefore, it is desired to induce DNA damage in tumor cells following the radiotherapy treatment. Accordingly DNA damage is non-desirable in healthy cells. Hence, enhancing DNA damage in tumors while protecting DNA in the healthy cells is a main objective of radiotherapy.

In order to increase the efficiency of radiotherapy, the mechanism of radiation-induced DNA damage must be well understood so that the radiation-induced DNA damage pathway can be well controlled.

1.2.1 Categories of radiation-induced DNA damage and its repair

Radiation-induced DNA damage can be characterized into several categories, depending on the location of the damage or depending on the origin of the damage. In the former case, major types of DNA damage are: base damage, strand breaks, abasic site, DNA-protein crosslinks and multiply damaged sites.

Base damage can be either caused by the direct or the indirect action of the ionizing radiation. The direct action of ionizing radiation may eject an electron from the unsaturated C-5 or C-6 position of the base. The resulting cation radical may further react with the hydroxyl ion to be deprotonated, forming a more stable species. On the other hand, in indirect action, it is traditionally believed that base damage is caused by hydroxyl radical attack on DNA bases through hydrogen abstraction or the addition of the hydroxyl radical on C=C unsaturated double bonds [11]. However, recent research done by our group utilizing

femtosecond time-resolved transient pump-probe laser spectroscopy to study the reaction of nucleotides has successfully shown that the prehydrated electron (see section 1.3 for details) generated from the radiolysis of water, is able to transfer themselves to the DNA bases through a dissociative electron transfer (DET) process [12]. We strikingly observed that the base G is most vulnerable to DET of e_{pre}^- leading to bond breaks, while the electron is most effectively captured by the base A to form a stable anion [12]. Similar to the attack by an oxidizing species, such a bond break at G may cause severe structural deformation and potential lesions to the DNA, as theoretically shown by Bera and Schaefer [13]. Base damage is one of the simplest forms of DNA damage and can be repaired through the base excision repair mechanism in mammalian cells. Unlike base damage, DNA strand breaks, especially double-strand breaks (DSBs), are much more lethal to the cells. Therefore, the prehydrated electron can induce both base damage and strand breaks in DNA through the DET process. Our findings have challenged the traditional notion that only the OH radical is the major contributor to DNA damage.

If the base damage is intense, it will lead to abasic sites. An abasic site is a location in DNA where neither a purine nor a pyrimidine base is present. Abasic sites include apurinic and apyrimidinic sites depending on the type of bases that are lost. Abasic sites also occur during the process of base excision repair as the endonuclease cleaves the bases before replacing them with the correct ones [14].

Moreover, damage to the deoxyribose-phosphate backbone may cause scission of the backbone and lead to the breakage of a DNA strand. If the breakage only occurs in one DNA strand, then it forms a single-strand break (SSB). Single-strand breaks are easily and quickly repaired by intracellular enzymatic processes, the detailed repair process will be discussed later. If the deoxyribose-phosphate backbone is damaged in two or more adjacent locations, then a double-strand break (DSB) will be formed. In order to form a double-strand break, it is pointed out that two adjacent single-strand scissions must not be more than 10 base pairs apart as the van der Waals forces and the hydrogen bonding between bases tend to hold the two single strands together [11,15]. Double-strand breaks may also be caused by a single energy deposition event from the direct action of LET (Linear Energy Transfer) radiation.

DSBs are difficult to repair since the DNA template required for damage restoration is not available anymore. Therefore, inducing DSBs in carcinoma cells under ionizing radiation is highly desired.

DNA-protein crosslinks can seriously affect DNA processing during DNA replication, transcription and even DNA repair. Many types of proteins such as structural proteins, transcription regulators, stress response proteins and cell-cycle regulatory proteins have been identified as being cross-linked to DNA. However, the role of DNA-protein crosslinks in overall radiation response has not yet been defined [11].

Energy from conventional ionizing radiation source such as x-rays is deposited unevenly in "spurs" and "blobs". Such energy distribution may lead to local multiply damaged sites. Multiply damaged sites are combinations of double-strand breaks and base damages.

Type	Yield
Single-strand breaks	1000
8-hydroxyadenine	700
T· (thymine damage)	250
Double-strand breaks	40
DNA-protein cross-links	150

Table 1-1 Measured numbers of damaged sites per cell per Gray (1 Gy = 1 J/kg). Table is reproduced from reference [14].

The final amount of DNA damage produced in the cells under ionizing radiation should be considered in terms of the cell's abilities to repair that damage. DNA repair mechanisms have been widely studied and several mechanisms are commonly acknowledged, they are base excision repair, nucleotide excision repair, mismatch repair, homologous recombination, non-homologous end joining (NHEJ), and error prone (SOS) repair [16].

Base excision repair takes care of the base damage in DNA. The mutated or damaged base will be removed from the DNA strand by a glycosylase enzyme, then the sugar residue will

be removed by an AP endonuclease. DNA polymerase will fill the vacancy with the correct nucleotide according to the complementary information on the opposite strand. Finally, the DNA strand is sealed by DNA ligase. Base excision repair mechanisms are fast and efficient as base damages occur frequently during normal DNA synthesis, replication and transcriptional processes. Therefore, base damages are not lethal to cells.

Nucleotide excision repair removes the bulk adducts formed in DNA. It is not lesion-specific as opposed to the base excision repair. In terms of radiation-induced DNA damage, nucleotide excision repair targets pyrimidine dimers that formed under UV-radiation. Though defective nucleotide excision repair does not lead to ionizing radiation sensitivity, researches have shown it increases the sensitivity to UV-induced DNA damage and certain anticancer drugs such as alkylating agents that induce bulky adducts.

There are two repair mechanisms responsible for fixing Double-strand breaks. They are homologous recombination repair and non-homologous end joining (NHEJ) repair. Homologous recombination repair is a high fidelity repair mechanism utilizing the undamaged homologous chromosome or sister chromatid as a template for DNA repair [16]. Homologous recombination repair primarily takes place in the late S/G_2 phase of a cell cycle, when sister chromatids are more easily available. In contrast, non-homologous end joining is error prone since the broken ends of DNA strands are simply processed and ligated together regardless of the original sequence of DNA. NHEJ probably accounts for many of the premutagenic lesions induced in the DNA of human cells by ionizing radiation.

The rest of the repair mechanisms are mismatch repair and the error prone translesion repair, both of which are not of great importance within the scope of radiobiology. Mismatch repair is able to remove the mismatched nucleotide during DNA replication, then replace the mismatch with the correctly base-paired nucleotide. The error prone translesion repair is highly error prone and may introduce more mutations to the cell [16].

DNA-protein cross-links repair mechanism is not yet well understood. Currently it is believed that a combination of nucleotide excision repair and recombination repair is needed

to repair DNA cross-links. Further details in this repair mechanism require future investigations.

The mechanisms of DNA repair have confirmed that among all radiation-induced lesions, DSBs are the most difficult to repair. *Hence, double-strand breaks and multiply damaged sites are the most relevant lesions in terms of radiation-induced cell death*. Double-strand break is the major factor that threatens the genomic integrity of the cell. If DSBs are insufficiently repaired, they may lead to chromosome breaks, deletions, and translocations [17]. Though the ability to repair DSBs vary among different cell types with 90% repair rate in radioresistant cell lines to less than 30% in other cell lines, generally DSBs are difficult to correctly repair [18].

1.2.2 Direct and Indirect Action

Ionizing radiation can cause damage in DNA through two major pathways: direct and indirect action. In direct action, the energy is directly deposited in the target DNA molecules without the intervention of radicals derived from water radiolysis. The targeted molecules or atoms will be directly ionized or excited, initiating a chain event that leads to biological effects. The direct action process is thought to be dominant under high linear energy transfer (LET) radiations, such as neutrons and α-particles [11].

On the other hand, indirect action is a major cause of DNA damage under low LET radiations (γ-ray, X-ray, etc.) [11]. In indirect action, DNA is attacked by the radiation-created radicals in the solvent, mainly by the radiolysis products of water because water constitutes 75-90% of the cell. Therefore, most radiation energy deposited in the biological system is initially absorbed by water, generating oxidizing and reducing radicals. The radiolysis products of water have long be considered to be e_{hyd}^- (the hydrated electron), $^\bullet OH$ (hydroxyl radicals) and $H^\bullet$, with G values (number of molecules produced per 100 eV) of 2.8, 2.4, 0.6 at 10^{-6} s after radiation, respectively [19,20]. It was thought that about two-thirds of the biological damage induced by x-ray irradiation is through indirect action from the OH radical, as determined by using OH radical scavengers [21,22].

Although DNA damage under ionizing radiation has been widely and intensely studied for decades, novel pathways of radiation-induced DNA damage have been found only recently. In direct action, it was found that the abundant low energy free electrons can cause DNA strand breaks through direct action [23]. In an aqueous cellular environment, however, indirect action pathway dominates. It was recently surprisingly observed that the weakly-bound (below-zero-energy) electron – the precursor states of the hydrated electron (or the prehydrated electron) – is an effective species inducing DNA damage through a reductive pathway [12,24].

1.2.3 Direct DNA damage caused by low-energy free electrons

For direct DNA damage pathway, depending on electron energy, electrons can induce DNA damage through ionization, dipolar dissociation (DD) and dissociative electron attachment (DEA) processes [25]. When a low-energy (<20 eV) free electron is attached to a molecule to form a temporary anion resonance, this process is called DEA [26]. If RH represents the DNA molecule, the electron produced from radiation energy deposition will attach to RH, forming a transient or stable molecular anion $RH^{\bullet-}$ [23]. The transient molecular anion will further dissociate along one or several specific bonds causing bond rupture through the formation of a radical and H^-:

$$e^- + RH \rightarrow RH^{*-} \rightarrow R^{\bullet} + H^- \text{ [23]}$$
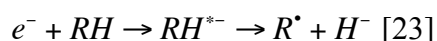
For the DEA process with a low-energy (0-20 eV) free electron, the intermediate transient anion is formed from the electron resonance attachment to the molecule. There are two types of resonance states: resonances that lie below the energy of their parent (the state from which they derive) are termed as the "Feshbach resonances" or "Type I resonances"; On the other hand, the resonances that lie above their parent states are "shape resonances" or "Type II resonances" [26].

In the Feshbach resonances, the electron affinity of the electronically excited state of the parent molecule is strong enough to maintain an incident electron. Such resonances cannot decay into the parent states when the excitation is near the center of the resonance. Therefore, new states with different configurations other than the parent states can be created from the

dissociation of the resonances. Feshbach resonances have longer lifetimes since the dissociation process involves changes in the molecular configurations [26].

Shape resonances arise when the incident electron occupies the previously unfilled orbital of the target molecule in its ground state. The incoming electron is trapped near the molecule by the electron-molecule potential barrier formed from nonzero electron angular momentum. In this case, the electron occupies the previously unfilled orbital of the molecule. In contrast with Feshbach resonances, it is energetically favourable for shape resonances to decay into the parent states, therefore, the shape resonances are short-lived species [26].

In the case of formation of DNA resonance states, both types of transient resonant anions can be created in the gas phase. The studies of low-energy-free-electron-induced DNA damage reported that with the electron energy above 10 eV, the Feshbach resonant anions occur [27], whereas with much lower electron energy, shape resonant anions are responsible for DEA to cause bond breaks. *However, in aqueous environment, the dissociative electron transfer reaction is the major process*. Details will be discussed later in the dissociative electron transfer (DET) sections.

Over the past decade, the direct DNA damage induced by low-energy free electrons has been studied both experimentally and theoretically. Low-energy (energy < 30 eV) electrons are abundant secondary electrons produced under ionizing radiation [28]. Electron-molecule interactions below 30 eV is described in terms of direct scattering or resonance scattering. Both pathways can potentially lead to direct DNA damage. Direct scattering occurs at all energy levels above the energy threshold and it produces a monotonic increasing DNA strand break yield function in terms of increasing electron energy. On the contrary, the resonance scattering is more characteristic with the formation of the transient anion at particular resonance energies, leading to a peak in the yield of DNA strand breaks.

The role of low-energy electrons has been unraveled since the 1990s. It was first proposed that the abundant secondary low-energy electron species produced along the radiation track are more biologically relevant both from experimental results or theoretical simulations. For example, Botchway et al suggested that low-energy electron species with energies 0.1 − 5

keV are most responsible for clustered damage in DNA under low-LET radiations [29]. Moreover, from computational modeling of ionizing radiation induced DNA damage in mammalian cells, Nikjoo et al attributed the largest percentage yield of double-strand breaks to the contribution of the secondary low-energy electrons with energies between 60 – 150 eV [30]. Ever since then, the energies of the effective low-energy electrons were found to be even lower. In 1999, experimental results reported that low-energy electrons with energies around 5 to 25 eV can damage biological molecules, like deoxyribose analogues and homo-oligonucleotides [31,32]. In 2000, the dissociative electron attachment to DNA was observed in dry supercoiled DNA in a high vacuum condition through the direct energy deposition on DNA molecules by 3-20 eV low-energy electrons, causing DNA SSBs and DSBs [23]. In 2001, the low-energy electron's attack on DNA bases (A, T, G, C) was evaluated by measuring the amount of fragmented anions produced by 5-40 eV LEE attack. All bases exhibit resonant peaks around 9 to 20 eV [33]. From these results, Abdoul-Carime et al concluded that LEEs induce DNA bond breaks by dissociatively attaching to the DNA bases. Pan et al further confirmed that dissociative low-energy electrons (LEEs) attachment induce DNA single and double stranded breaks by observing the yield dependence of desorption anions on the incident electron energy, which clearly shows a DEA signature peak around 9 eV [34]. However, the initial experiments were not able to identify specific DNA components (sugar, phosphate group and DNA base units) that are responsible for the strand breaks induced by LEEs since these basic DNA constitutes can all be fragmented via DEA between 5 and 13eV [35].

Subsequently, in order to better understand the exact location of bond rupture by DEA of the low-energy electrons, a number of studies have been carried out on electron interactions with isolated nucleic acid base molecules or isolated nucleotides in the gas phase. The electron attachment to gas-phase uracil, adenine, cytosine, sugar analogs and phosphate groups have been studied extensively [27,32,36-62]. For example, theoretical calculations have shown that cytosine bases are capable of capturing electrons with energies even below 1 eV to form a π^*-anion state, which can further cause a "phosphate-sugar O-C σ bond cleavage" [38,63]. Berdys et al also pointed out that within a model solvation environment, a

12

significant fraction of the LEE-induced π^*-anion state is likely to become electronically stable, indicating the dissociation is less probable to occur [63]. These results were further verified by theoretical work done on pyrimidine nucleotides, which found that electronically stable radical anions could form from attachment of near-0-eV electrons in both gas and aqueous solutions [53]. Another theoretical research project explored the exact location of the C-O bond cleavage proposed in pyrimidine nucleotides. They found $C_{3'}$-$O_{3'}$ bond cleavage dominates because of its lower activation energy [61]. Moreover, Gu et al postulated that LEE-induced DNA damage may not occur in aqueous environment due to the polarization effect which increases the activation energies of all kinds of bond breaks [61]. On the other hand, electron attachment to purine bases have been observed as well. For example, base damage to gas-phase adenine induced by low-energy electrons was reported from experimental studies [51,52,56,64]. There are some interesting findings about guanine bases. Photoemission electron spectroscopy experiments performed on dry DNA oligomers show that in the single-strand DNA oligomers, the capturing probability of low-energy electrons scales with the number of G bases [65]. Whereas theoretically, G base is likely to have N-H bond dissociation to induce bond breaks [13]. Other results with sugar analogues and phosphate groups have shown that excision of ribose containing C5 is sensitive and deoxyriboses quite fragile to LEE attachment, whereas phosphate groups have two low energy electron resonant features at 1 eV and 8 eV [66,67]. These results argued for a mechanism of SSBs induced by LEEs. However, other researchers argue that direct LEE-attachment to sugar and phosphate groups are not as feasible due to a higher energy barrier [38]. Moreover, the electron attachment cross-sections have been calculated for both single-strand breaks and three bases (adenine, thymine and cytosine) [45]. The electron attachment cross-sections for those three bases are about 3-10 times smaller than the cross-sections of SSBs. Therefore, it is concluded that base damage is less likely to occur than strand breaks in low-energy electron induced DNA damage. Martin et al studied supercoiled DNA bond breaks induced by 0-4 eV electron shape resonances. They conclude that SSBs are enhanced by ~1 eV electron attachment but no DSBs are induced by 0-4 eV electrons [68].

One can see that studies done by different groups often yielded rather contradictory results regarding the mechanism of the LEE-induced DNA strand breaks in terms of efficient electron energies, locations of damage and cross sections of nuleobases to LEE attachment. The detailed mechanism still needs to be elucidated. Overall, the generally-agreed mechanism of LEE-induced DNA strand breaks states that DNA bases first capture LEEs to enter π^*-anion shape resonance states, with a subsequent electron transfer to the backbone to cause either C-O bond cleavage or glycosidic bond breaking, producing the corresponding phosphoric anions and deoxyiribose radical fragments. Thus a strand break is formed.

Theoretical researchers have investigated DEAs to nucleotides in both gas-phase and aqueous solutions [55,61,63,69]. But none of the experiments regarding LEE-induced DNA damage were performed in real aqueous solution: above experimental observations were all done in a gas-phase condition with dry biological samples. As mentioned previously, indirect DNA damage dominates over the direct DNA damage under ionizing radiation. Experiments have shown that the yields of DNA strand breaks (single-strand breaks and double-strand breaks) induced by γ-ray radiation in an aqueous environment are three orders higher than those in a dry condition [70]. Though some authors claim that on average there are 2.5 water molecules remaining for each base pair as its structural water when DNA samples are prepared under the UHV (ultrahigh vacuum) condition [34], this amount of water is far less than that present in a cellular environment. In a biological cell, DNA molecules have at least two hydration shells around them. The first hydration shell alone consists of around 20 to 30 water molecules per nucleotide [71-73]. Moreover, some theoretical research aimed to explore LEE-induced DNA strand breaks in aqueous environment reported that a polarized aqueous environment is likely to quench the actions of the low-energy electrons by increasing the activation energy barrier for bond cleavages [55,61,63,69]. Furthermore, the water environment cannot enhance the dissociative electron attachments (DEA) of molecules involving free electrons with energies greater than 1.0 eV. It has been observed that the polar environment of H_2O/NH_3 ice can completely quench DEAs of many molecules with > 1.0 eV free electrons though those DEAs are effective in gas-phase [74-77]. Therefore, the water environment is likely to protect DNA molecules from low-energy electron induced direct

DNA damage at energies above 1.0 eV. *On the other hand, the presence of water can significantly enhance the capture of ~ 0 eV electrons and the associated dissociation of molecules..* This can be explained by the dissociative electron transfer mechanism as detailed in the next section.

1.3 Reductive Radiation-Induced DNA Damage by prehydrated electrons

The fact that water is the main constituent in the human body makes it impossible to neglect the role of water molecules under ionizing radiations. About 75 – 90 % of a cell is made up of water. Therefore, water molecules absorb the majority of the radiation energy deposition in cells initially. It is well known that the indirect radiation-induced DNA damage caused by the radicals produced from the radiolysis of water dominates over the direct DNA damage induced by the energy deposition at DNA itself. Indeed, *it has been observed that the yields of the single-strand breaks and double-strand breaks of DNA produced by γ-ray radiation are three orders higher under the aqueous condition than those in a dry condition* [70]. This fact clearly shows that water has a crucial role in enhancing the radiation-induced DNA damage. The key question then lies in how the radiolysis of water leads to DNA damage. Depending on how high the deposited energy is, the water molecules can be either ionized or excited. Ionization or excitation of water molecules generates an oxidizing $^{\bullet}$OH radical, a free electron, as well as a hydrogen radical. For example, under ionization:

$$
\begin{aligned}
&H_2O \rightarrow H_2O^+ + e^- \\
&H_2O^+ + H_2O \rightarrow H_3O^+ + {}^{\bullet}OH
\end{aligned}
\tag{1.1}
$$
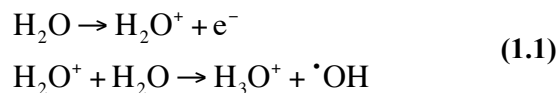
Here, the term radical is referring to an atom or group of atoms containing an unpaired electron, which is highly reactive.

Under excitation, water molecules will also produce radicals and ejected electrons as shown in the following reactions:

$$
\begin{aligned}
&H_2O \rightarrow H_2O^* \\
&H_2O^* \rightarrow H^{\bullet} + {}^{\bullet}OH \text{ or } H_2O^+ + e^-
\end{aligned}
\tag{1.2}
$$
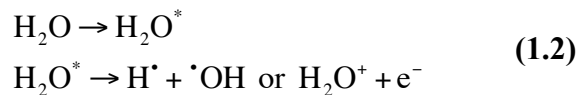
The ejected free electron will quickly be trapped by the surrounding water molecules to become a prehydrated electron and finally a hydrated (solvated) electron in a potential well:

$$e^- + nH_2O \rightarrow e^-_{pre} \rightarrow e^-_{hyd} \qquad (1.3)$$
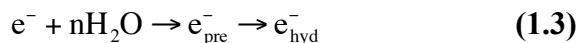
The hydrated electron belongs to the large family of solvated electrons. When the solvated electron is formed in water, it is termed as the hydrated electron (e_{hyd}^- and e_{aq}^-). The proposal of the solvated electron dates back to more than a century ago. Nearly 200 years ago, it was found out that in ammonia vapor, potassium metal becomes gold and blue [78]. Similarly, all alkali metals in liquid ammonia are brightly coloured when the solution is dilute, whereas the concentrated solution (> 3 M) presents copper colour. In 1907, Charles Kraus explained the production of the bright colour by introducing the concept of a "solvated electron" [79,80]. He proposed that the alkali metal ionizes in liquid ammonia, forming a cation and a solvated electron. Though the solvated electron is stable in ammonia for days, it has a very short lifetime in water. Therefore, owing to its short lifetime (~200 ns) in water, the hydrated electron was not confirmed until 1962, when its optical spectrum was successfully measured by E.J. Hart using the pulse radiolysis technique [81]. Subsequently, e_{hyd}^- is recognized as one of the primary radicals formed upon the radiolysis of water.

The structure of the hydrated electron has been studied through many theoretical approaches, such as the model for quantum molecular dynamics (MD) simulations in the liquid phase, density functional theory study and dynamical polaron theory [82-84]. Among those theoretical studies, the quantum molecular dynamic model provides a relatively simple approach and the closest simulation to experimental observations [83]. From MD simulations, it states that the water cluster conformation formed around the hydrated electron consists of two solvation shells; the first solvation shell is composed of approximately six water molecules with their OH bonds, in which H atoms bear partial positive charges, directed toward the electron, forming a "cavity" [83]. The cavity model has been used to describe the hydrated electron for more than 40 years. Generally in this model, the electron stays in the cavity to avoid the regions where the water molecules have large electron density. The cavity is stabilized by the charge interactions with the dielectric medium, which

in this case is the water molecule. Though cavity model has been around for decades, in the past two years, this popular model of the hydrated electron has been challenged [85-87]. The exact conformation of the hydrated electron is still under investigation.
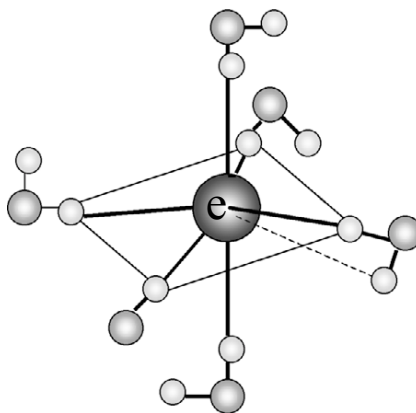
Figure 1.1 Schematic diagram showing the cavity model of a hydrated electron [11]. The first solvation shell of the hydrated electron consists of six water molecules. Together they form a "cavity" around the electron [83].

For over 40 years, the main radiolysis products of water were known to be the hydrated electron (e_{hyd}^-), the hydroxyl radical ($^\bullet$OH) and a hydrogen radical (H$^\bullet$) with quantum yields (G values) of 2.8, 2.4 and 0.6, respectively, at 10^{-6} s after the radiation event under x-ray ionizing radiation. Hence, for conventional ionizing radiation sources such as x-rays and γ-rays, the yield ratio of $^\bullet$OH radicals and the hydrated electron e_{hyd}^- is generally accepted as r = [$^\bullet$OH]:[e_{hyd}^-] ≈ 1:1. In this case, the ionizing process of water molecules, as described in Equation (1.1), dominates over the dissociation process (as described in Equation (1.2)). The dissociation process is likely to produce the $^\bullet$OH rather than the e_{hyd}^-. Therefore, under conventional ionizing radiation sources, the hydrated electron has the highest quantum yield among all the radiolytic products of water.

Though the hydrated electron has the highest quantum yield, it is deeply trapped in the water cavity at ~3.2 eV below vacuum level [88]. As a result, this ground-state-like hydrated electron is ineffective at inducing DNA damage. Therefore, the $^\bullet$OH radical has been considered as the sole contributor to radiation-induced indirect DNA damage. However, one third of the DNA damage is not scavengable by a high-concentration OH radical scavenger

17

[89]. If that one-third non-scavengable DNA damage were attributed to direct DNA damage [11,89], then it would contradict to the fact that water can enhance radiation-induced DNA damage by three orders of magnitude [70]. Indeed, how radiolysis products of water induce DNA damage has been a long-standing mystery. Understanding the exact role of water in radiation-induced DNA damage can shed light on possible pathways to improve radiotherapy efficiency.

With the advent of ultrafast laser spectroscopy techniques, the ultrafast hydration process of electrons in liquid water has been studied intensely. The precursor state of the hydrated electron, denoted as the prehydrated electron (e_{pre}^-) was discovered. Though the existence of the precursor states of the hydrated electron had been implied in many early studies [90-92], the first evident observation was made in 1987 by Migus et al using femtosecond laser spectroscopy [93]. Since then, the physical and chemical properties of the ultrashort-lived prehydrated electron have been studied extensively [94-101]. The localization of an excess electron in water was found to proceed with the p-like prehydrated electrons and then the s-like hydrated electron state. In contrast to the lowest s-like hydrated electron, which is deeply trapped in the water cavity at ~-3.2 eV below the vacuum level and has a long-lived lifetime on the μs-ns scale, the prehydrated electrons are weakly bound at ~-1.5 eV and have an ultrashort lifetime below 1 ps. The lifetimes of the prehydrated electrons were reported to range from 50 fs to 1 ps [82,93,94,97,99,102-105]. However, with the careful Femtosecond Time-Resolved Pump-Probe Laser Spectroscopic (fs-TRLS) measurements, our group [101] resolved the controversies that had existed for over two decades. Wang et al. [101] directly detected the rise and decay of the prehydrated electron produced from the two-photon excitation method of water molecules. They identified and removed an artificial effect of the coherence spike caused by the spatial and temporal overlaps of pump and probe pulses from the real electron signal. This coherence artifact in the femtosecond pump-probe experiments have been studied both theoretically and experimentally [101,106-109]. It was demonstrated that the ultrafast rising times at tens of femtosecond observed in previous studies were due to this coherence artifact [101]. After removing the spike effect, Wang et al's results yielded two intrinsic states of prehydrated electrons with lifetimes of 180 ± 30 fs and 545 ± 30 fs

[101]. These lifetimes are consistent with the experimental results reported previously by Eisenthal's group and Laubereau's group [94,97,110], and the theoretical simulations by Rossky and co-workers [111].

The fact that the prehydrated electron is only weakly bound to the water molecules implies the high reactivity of the prehydrated electron. Indeed, the high reactivity of the prehydrated electron attracted various interest in the past two decades. The prehydrated electron has been observed to play an essential role in environmentally, chemically and biologically important reactions. For environmental significance, for example, Lu, Madey and Sanche have shown that e_{pre}^- is responsible for the dissociation reaction of chlorofluorocarbons (CFCs) in the atmosphere, which leads to a new ozone-hole formation theory [75-77,98,112-115]. Lu has recently found that CFCs, which are also strong greenhouse gases, have made a major contribution to the earth temperature change since 1950s [116]. In biological systems, e_{pre}^- can efficiently attach to biological molecules, such as amino acids and nucleotides [117,118]. More recently, using our state-of-the-art fs-TRLS, our group has observed the dissociative electron transfer (DET) reactions of e_{pre}^- with anticancer drugs and DNA: e_{pre}^- can activate chemotheraputic drug cisplatin (CDDP) [119,120] and potential radiosensitizers — halopyrimidines (CldU, BrdU, and IdU) through the dissociative electron transfer (DET) process [121-123]. For the transfer of e_{pre}^- to nucleotides dXMP (where X is one of the four nucleobases: adenine A, thymine T, guanine G or cytosine C), it leads to bond breaks of T and especially G bases, while it results in stable anions of C and especially A. Among all four types of mononucleotide, the guanine mononuleotide is the most vulnerable to DET process, implying that nucleotides containing guanine are the weakest link in DNA [12]. Indeed, such an observation is consistent with the experimental results by Ray and co-workers, which show that dry single strand DNA oligomers with more G bases have higher probability to capture low energy electrons (~1.0 eV) in gas phase [65], and with the experimental result by Liu et al that water clusters can protect the collision induced dissociation of anionic adenosine 5'-monophosphate (AMP-) [124]. Theoretical studies by Shaefer et al found that the G base is likely to have N-H bond dissociation to induce bond breaks, which supports our findings as well [13]. Compared with these previous studies, our

19

group's results provided the *first real-time* observation of the dissociative electron attachments of G and T and the formation of all four stable anions (A⁻, G⁻, C⁻ and T⁻), particularly in aqueous solution [12]. These results have revealed that the DET reaction of e_{pre}^- is a key step in radiotherapy. The reaction of e_{pre}^- with DNA leads to the study of reductive pathway of DNA damage. Therefore, the prehydrated electron is an ideal species to study reductive DNA damage.

Oxidative DNA damage induced by the hydroxyl radicals have been well-studied for decades. But little is known about the reductive DNA damage induced by prehydrated electrons. The prehydrated electron interacts with DNA molecules through the DET process. First, it has been observed on H_2O/NH_3 ice surfaces that the water environment significantly enhances the cross sections for DEA of molecules with electrons at energies ~0 eV, whereas DEAs with > 1.0 eV electrons are completely quenched [74-77]. The enhancement is due to the DET mechanism [12,20,75,77,98,101,112,113,121,122]. The electrons with ~0 eV energies are first trapped by the polar water molecules to form the prehydrated electrons. An e_{pre}^- is then transferred to a molecule, leading to the dissociation of the molecule. Second, It has been shown that DEAs for near 0 eV electrons in the gas phase can shift to lower energy levels of about -1.0 ~ -1.5 eV in polar liquid solutions because of the polarization effect. As observed for halopyrimidines,and CCl_4 [121,122,125], the lowered energy levels match the energy level of e_{pre}^-, leading to effective Feshbach resonances. Therefore, the effective DETs of the halopyrimidines and CCl_4 molecules with e_{pre}^- were observed. Third, effective DET reactions of e_{pre}^- with DNA bases especially G have similarly been observed [12]. The DET processes of e_{pre}^- can induce double-strand breaks in DNA by inducing bond dissociation on one strand, and then the dissociation products can further break the other strand [12]. Moreover, low-energy free electrons produced under ionizing radiation have extremely short residence times (on the scale of one tenth to a few femtoseconds) in water and they are quickly thermalized into the weakly-bound prehydrated electrons with energies below 0 eV [93,94,97,101,110,111]. Overall, in real cellular aqueous environments, it is the prehydrated electron rather than the low-energy free electron that plays the dominant role in inducing DNA damage.

20

Indeed, in our recent studies, we have observed reductive DNA damage induced by the prehydrated electron. Our novel result proved that not only does the prehydrated electron produce DNA damage, it is in fact quite effective at producing the damage. We found that the e_{pre}^- is at least twice as effective as the hydroxyl radical at inducing DNA damage through the reductive pathway [24]. Hence, studying the reductive DNA damage caused by the e_{pre}^- can shed light on detailed mechanism of radiation-induced DNA damage, leading to improvements of radiotherapy.
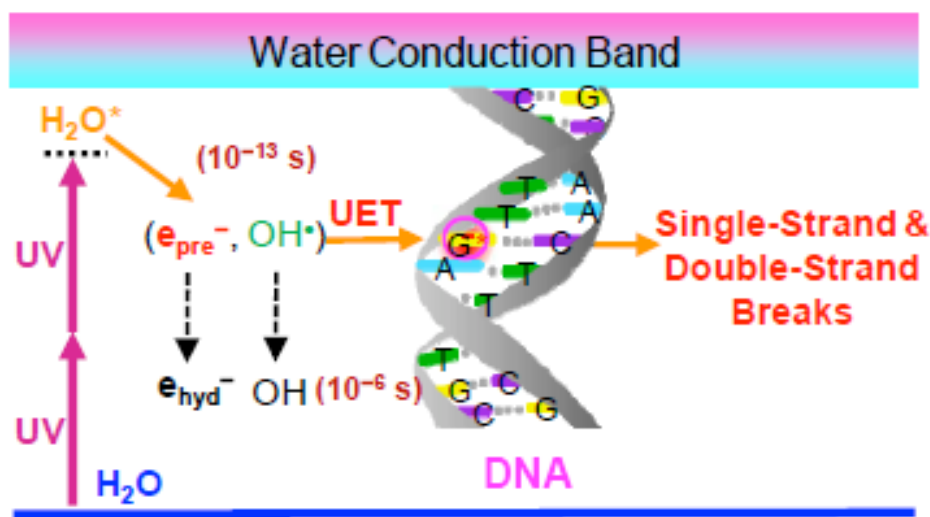
Figure 1.2 Two-photon excitation of water molecules at wavelength of 266 – 380 nm, producing the e_{pre}^- and OH radicals within 10^{-14} s. These radicals attack DNA strands to cause single-strand and double-strand breaks [24].

1.4 Objectives of the Project

In order to further study the role of the prehydrated electron in the reductive DNA damage pathway, additional chemical compounds have to be used to regulate the prehydrated electron. The chemical compounds that can efficiently react with the prehydrated electron are termed electron scavengers. Potassium nitrate (KNO_3) is such an electron scavenger. Therefore, the goal of our project was first to study the effectiveness of potassium nitrate as an e_{pre}^- scavenger, in order to apply KNO_3 for cellular experiments. Second, we also aimed to quantitatively determine the scavenging reaction efficiency of KNO_3 with the e_{pre}^-.

Moreover, since it is important to compare the efficiency of the reductive DNA damage induced by prehydrated electrons to that of the oxidative DNA damage induced by $^\bullet$OH radicals quantitatively, $^\bullet$OH scavengers will be applied in the biological experiments to leave the prehydrated electron as the only active species. However, no one has reported if the $^\bullet$OH scavengers scavenge the prehydrated electron. Therefore, another part of my project is to study the possible reactions between $^\bullet$OH scavengers (isopropanol and DMSO) and the prehydrated electron. If there are scavenging reactions, then the efficiency of such reactions will be determined quantitatively.

Furthermore, knowing the yield ratio of $^\bullet$OH and the e_{pre}^- (r = [$^\bullet$OH]/[e_{pre}^-]) can facilitate the direct comparison of $^\bullet$OH and the e_{pre}^- at inducing DNA damage. Hence, we intended to use an $^\bullet$OH scavenger KSCN to capture $^\bullet$OH radicals. Their reaction product absorbs strongly in the visible region. Detecting the reaction product of KSCN and $^\bullet$OH radicals and knowing its extinction coefficient can help the study of not only the reaction dynamics of $^\bullet$OH radicals, but also the amount of $^\bullet$OH radicals produced compared to the amount of e_{pre}^-. Therefore, the yield ratio r will be obtained in my project for two-photon UV excitations of water.

1.5 Scope of the Thesis

Following this introduction, the principle of time-resolved femtosecond (fs) laser spectroscopy is introduced in chapter 2. Chapter 3 presents direct observations of the ultrafast electron transfer reactions of the electron scavenger KNO_3 with the prehydrated electron. The quantitative analysis of the scavenging efficiencies is addressed. The experimental studies of the ultrafast electron transfer reactions extend to the scavenging reactions of $^\bullet$OH radical scavengers with the prehydrated electron in chapter 4. Quantitative analysis is present and the ultrafast behaviour of the prehydrated electron is confirmed once more. In chapter 5, with the aid of an $^\bullet$OH radical scavenger potassium thiocyanate (KSCN), the reaction dynamics of $^\bullet$OH radicals and KSCN is studied, from which the properties of $^\bullet$OH radicals are derived. The quantum yield ratio of the $^\bullet$OH radical and the prehydrated electron is obtained to assist the direct comparison of the biological effectiveness of $^\bullet$OH radicals and prehydrated

electrons at causing radiation-induced DNA damage. Finally, the conclusions are summarized in chapter 6.

Chapter 2
Experimental Techniques

The major experimental technique applied in this project was Femtosecond Time-Resolved Pump-Probe Laser Spectroscopy. Femtosecond Time-Resolved Pump-Probe Laser Spectroscopy (fs-TRLS) was first introduced into the ultrafast chemistry field by Nobel Prize Laureate A.H. Zewail in late 1980s. Now it is widely used for observation of femtosecond scale chemical reactions.

2.1 The Importance of Using Femtosecond Resolution
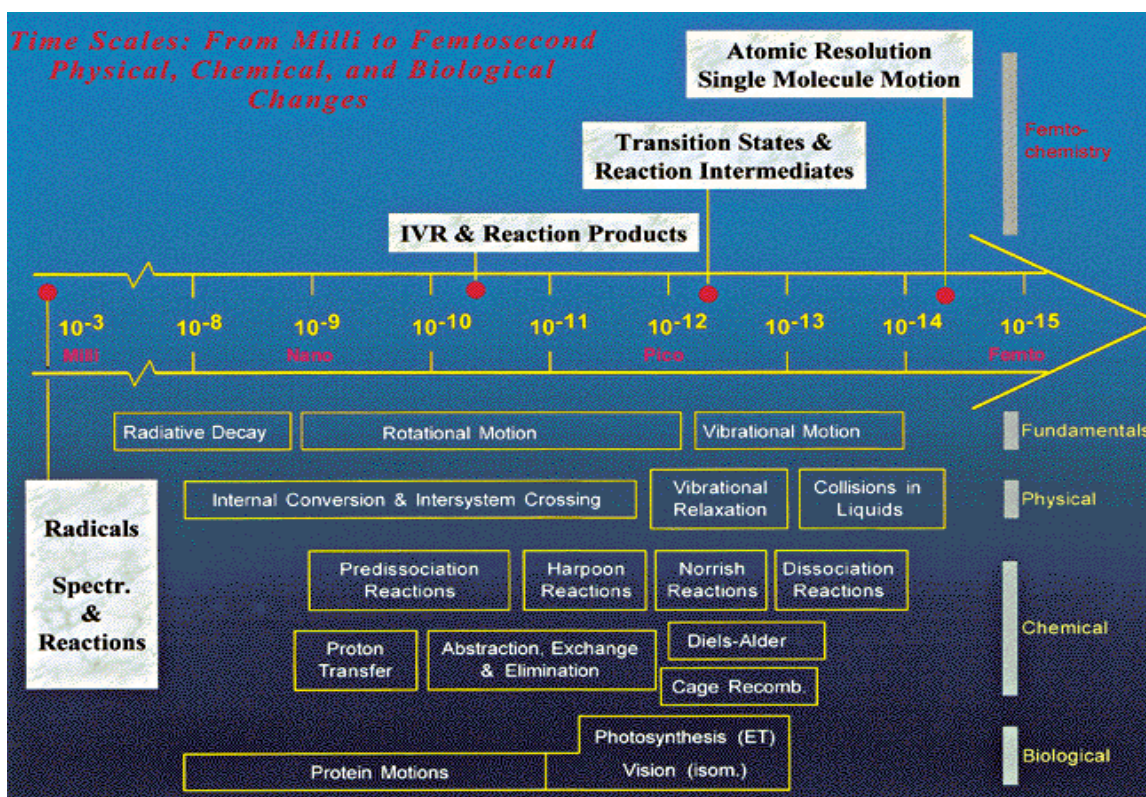

Figure 2.1 The time-scale diagram of the basic physical, chemical and biological changes [126].

Before the fs-TRLS technique, the pulse radiolysis method that can probe chemical reactions at the microsecond level was already widely used. But the microsecond time domain was not refined enough for studying the chemical reactions in details. Better time resolution with

femtosecond time scale was desired. Why was femtosecond necessary? As one can see from Figure 2.1, where the time-scale of the basic physical, chemical and biological changes are summarized, chemical bond breaking or bond formation occur rapidly, often in less than 1 ps (10^{-12} ps). It was one of the fundamental problems in chemistry to understand how those ultrafast events determine the entire course of the reaction [127]. Moreover, the biological changes that appear at longer time scales are often initiated by the fast processes at earlier times. The relatively slow biological processes such as DNA damage and cell death that take microseconds or longer, are often triggered by fast processes at earlier time [20]. Often, those fast processes lead to the formation of reactive radicals. One may argue that since the interactions are initiated by radicals and radicals often have long lifetimes covering from nanoseconds to even microseconds, then why are the biological processes initiated by processes much faster than nanoseconds? The answer is, though the radical might be long-lived, the formation of these radicals are ultrafast events that can happen faster than a picosecond [126]. Hence, in order to get a complete picture of the biological events, one must apply advanced physical methods with femtosecond resolution to study the biochemical reactions that occur in the ultrafast time domain.

The advent of the femtosecond time-resolved pump-probe laser spectroscopy provides us with the ability to capture the ultrasfast process within femtoseconds. Through this technology, we can finally take "motion pictures" of the rapid biochemical reactions.

2.2 Femtosecond Time-Resolved Pump-Probe Laser Spectroscopy (fs-TRLS)

Figure 2.2 illustrates the basic set-up of the femtosecond time-resolved pump-probe laser spectroscopy. In this technique, an ultrafast laser is used to generate a femtosecond width laser pulse. This laser pulse is split out into two parts: one as a pump pulse and the other as a probe pulse. Both of the laser pulses are sent to nonlinear optical devices, such as optical parametric amplifiers (OPA) to obtain the desired frequency. The pump pulse excites the reaction by initiating the sample molecules or electrons to excited states through photon excitation. For instance, in order to study the prehydrated electron dynamics, the pump pulse excites water molecules in the sample through two-photon excitation process. When the

pump pulse arrives at the sample, the experimental clock is set to zero. The probe pulse reaches the sample several femtoseconds or picoseconds after the pump pulse. The probe pulse records a snapshot of the reaction at that particular instant by examining the absorbance of the probed species through the measurement of the transmitted intensity of a probe pulse. The measured absorption signal is the difference between the intensities of the transmitted probe pulse in the presence and absence of the pump pulse [129].
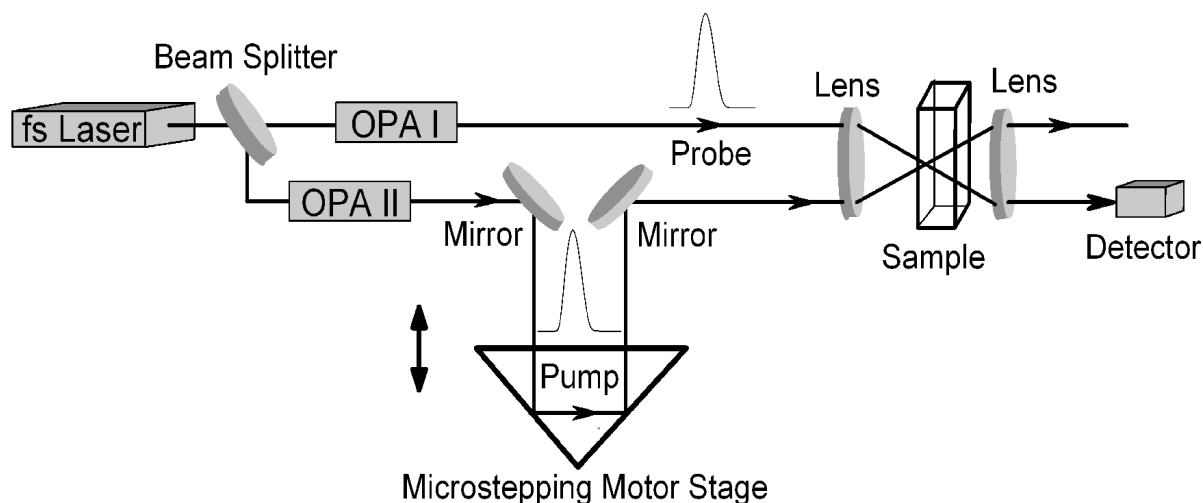
Figure 2.2 Schematic Diagram of Pump-Probe Absorption Spectroscopy [128].

During chemical reactions, different intermediate species have their own absorption bands. By monitoring probe wavelength, absorption behaviours of different intermediate species can be examined. The time-resolved absorption behaviour is observed by controlling the timing of the pump pulse and the probe pulse. One of the two pulses, for example, the pump pulse is sent over an optical path whose length is adjusted by moving a mirror on a mircostepping motor stage. Hence by changing the optical path difference (OPD) between the two pulses, the delay time is varied accordingly. For an OPD of 1 μm, the corresponding time resolution is:

$$\Delta t = \frac{\Delta s}{c} = \frac{1\,\mu m}{3 \times 10^8\,m/s} = 3.3\,fs \quad \textbf{(2.2.1)}$$

Where c is the speed of light in vacuum. Thus, the femtosecond time resolution is achieved. By altering the time delays between the pump and probe pulses continuously, many snapshots of the reaction can be taken at different time intervals. Therefore, if these snapshots are linked together, a "movie" of the reaction can be produced, which is a time-resolved transient absorption spectrum.

2.3 Experimental Setups

In our femtobiology/femtomedicine group, the pump-probe laser spectroscopy is utilized with a Ti: sapphire laser system. The Ti: sapphire laser system is able to produce 100-120 fs, 1 mJ laser pulses centered at 800 nm with a repetition rate of 1 kHz. Pump and probe pulses are generated from two optical parametric amplifiers (OPA), which are capable of producing pulses with wavelengths from ultra-violet (UV, $\lambda \geq 266$ nm) to near infrared (NIR, a few micrometers). The polarization angle of the pump and probe pulses were set at the magic angle 54.7° to avoid the contribution from polarization anisotropy due to the rotational diffusions of the molecules [130,131].

The pump pulse was chosen at 266, 318, 330 and 400 nm to excite water molecules, thus generating the prehydrated electron. The energy of the pump pulse used in all experiments was between 80 nJ to 440 nJ. While the probe wavelength was chosen at 635 and 800 nm to probe the absorption signal of equilibrated hydrated electrons or 480 to probe the dimer radical anion ((SCN)$_2^{\bullet-}$). The power detectors of the probe signal as well as the microstepping motor stage were both connected to the computer and feedback information was given to a labVIEW program. Hence real-time observations of electron transient absorption kinetic traces are displayed in the labVIEW program.

All transient absorption traces were measured at room temperature (between 295.5 K and 296.5 K). All the liquid solutions were put in a 5 mm quartz cuvette with a constantly stirring magnetic bar to avoid accumulation of reaction products.

Ultrapure water with a resistivity greater than 18 MΩ/cm, and the organic content < 1ppb obtained directly from a Barnstead Nanopure water system was used.

Chapter 3

Direct Observation of the Prehydrated Electron with an Electron Scavenger

3.1 Introduction

Potassium nitrate (KNO_3) has long been known as an effective hydrated electron scavenger with a high scavenging efficiency of 9.7×10^{11} $M^{-1}s^{-1}$ [19]. As the high reactivity of the prehydrated electron was unraveled, it is reasonable to infer that potassium nitrate may capture these excited states of the hydrated electron effectively. Moreover, quantitative knowledge of the scavenging reactions of the prehydrated electrons is required when using the electron scavenger to study the action of the e_{pre}^-. Hence, in this chapter we present a study of potassium nitrate with these excited states of the hydrated electron.

3.2 Experimental Details

We utilize the advantage of fs-TRLS to obtain real time observations of the scavenging reaction dynamics. The pump pulse was chosen at 318, 330 and 400 nm to excite water molecules, thus generating the prehydrated electron via two-photon excitation at 318 or 330 nm and three-photon excitation at 400 nm of water molecules. The energy of the pump pulse used in all experiments was between 80 nJ to 440 nJ, depending on the laser conditions, to achieve optimal signal. While the probe wavelength was chosen at 635 and 800 nm to probe the absorption signal of equilibrated hydrated electrons. The power detectors of probe signal as well as the microstepping motor stage were both connected to the computer and feedback information was given to a labVIEW program. Hence electron transient absorption traces are directly displayed by the labVIEW program.

Potassium nitrate from EMD™ was used as supplied. Ultrapure water with a resistivity greater than 18 MΩ/cm was obtained from an ultrapure water system (Barnstead's Nanopure) with <1 ppb total organic content, which was used in all sample solutions. All sample solutions were held in a 5 mm quartz cuvette with a magnetic stirring bar to avoid any photoproduct accumulation. All static one-photon absorption spectra were taken using a

UV/visible spectrophotometer (Beckman, Life Science). All experiments were performed at room temperature.

3.3 Determination of extinction coefficients for KNO_3

Since the pump-probe spectroscopy involves photon excitation, the absorption of KNO_3 itself to the pump pulse must be taken into account. Hence, the static absorption spectrum of KNO_3 needs to be studied. Beer-Lambert Law states that the light transmitted through a substance decays exponentially with respect to the concentration of absorbing species, the transmission path length and the extinction coefficient. In liquid, Beer-Lambert Law follows:

$$T = \frac{I}{I_0} = 10^{-\varepsilon l c} \qquad (\textbf{3.1})$$

Where T is the transmission of light I_0, l is the path length, c is the concentration of absorbing species, ε is the extinction coefficient (or molar absorptivity) and it normally has a unit of $M^{-1}cm^{-1}$. The quantity absorbance is then defined as:

$$A = \varepsilon l c \qquad (\textbf{3.2})$$

Hence, from static absorption spectrum (absorbance A), ε can be determined according to equation 3.2.

The absorption spectrum of KNO_3 is measured in a UV/Visible/NIR spectrophotometer (Beckman, life sciences) with the concentration from 0.1 M to 0.5 M and 0.1 to 1.0 M for 318 nm and 330 nm, respectively. The absorption spectrum is obtained within wavelengths of 190 nm and 450 nm. The absorption spectrum of 0.1M KNO_3 is demonstrated in Figure 3.1.

The extinction coefficient is extracted from Figure 3.1 by dividing A with path length l =0.5 cm, c =0.1 M. The extinction coefficient is plotted from 250 nm to 400 nm in Figure 3.1. Clearly, for the pump wavelength at 318 nm and 330 nm, the extinction coefficient is not zero, which means the absorption of the pump pulse from KNO_3 must be considered. By measuring the static absorption spectra from 0.1 M to 1.0 M KNO_3, extinction coefficients at 318 and 330 nm can be determined. These coefficients are determined by plotting the

absorbance at 318 and 330 nm versus the concentration, which leads to a linear function as in Figure 3.2. The slope denotes the product of ε and l. Hence the extinction coefficient is determined as $\varepsilon_{318} = 2.9$ M^{-1}cm^{-1} and $\varepsilon_{330} = 0.77$ M^{-1}cm^{-1} for 318 and 330 nm, respectively.
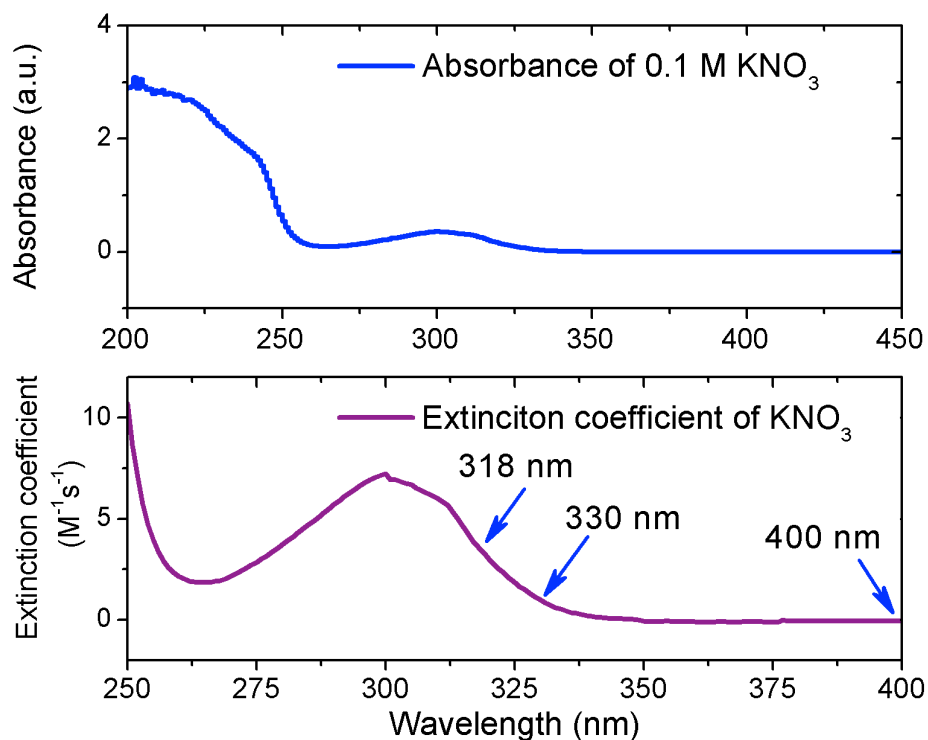
Figure 3.1 The static absorption spectrum of KNO$_3$.

3.4 Transient Absorption Kinetic Traces of e$_{hyd}^-$

3.4.1 Transient Absorption Kinetic Traces

In general, there are two approaches to study the dynamics of the prehydrated electron through the femtosecond time-resolved laser spectroscopy: one is to directly monitor the transient absorptional traces of the e$_{pre}^-$ by probing its absorption in the infrared region; the other is to monitor the transient absorptional traces of the e$_{hyd}^-$ in the visible region, then the initial yield of the hydrated electron is equivalent to the quantum yield of the prehydrated electron since the prehydrated electron will thermalize into the hydrated electron, giving rise to e$_{hyd}^-$ signal. In this way the prehydrated electron yield can be derived. The two approaches

31

are essentially equivalent. In our project, because it is more convenient to produce laser pulses in the visible region, we adopted the second approach.
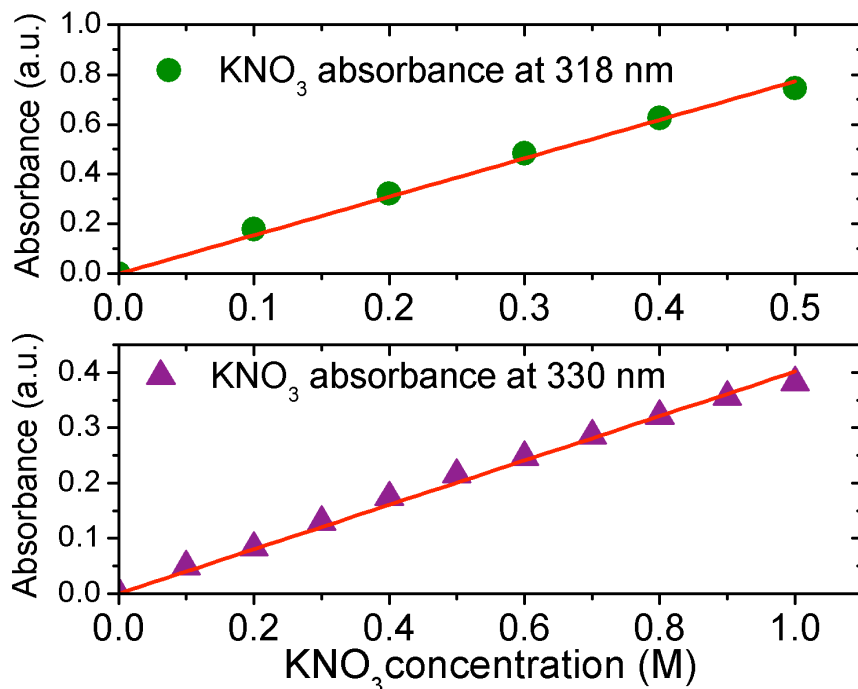
Figure 3.2 Extinction coefficients of potassium nitrate determined at 318 and 330 nm.

The pump pulse is chosen at 318, 330 and 400 nm to excite water molecules through the two-photon (318 and 330 nm) or three-photon (400 nm) excitation processes, in order to produce the major water radiolysis radicalss (OH radical and e_{pre}^-).As illustrated in Figure 3.3, the prehydrated electron states are the excited states of the hydrated electron. The absorption of the hydrated electron at the 720 nm (1.7 eV) wavelength corresponds to the transition from the hydrated electron (-3.2 eV) to the prehydrated electron (-1.5 eV) as shown in Figure 3.3. The extinction coefficient of the hydrated electron is plotted in Figure 3.4. For probe wavelengths 635 and 800 nm, the hydrated electron presents large extinction coefficients around 17500 $M^{-1}s^{-1}$ [19]. Therefore, at those wavelengths, we can detect the transient absorption traces of e_{hyd}^- in order to derive the dynamics of e_{pre}^-.
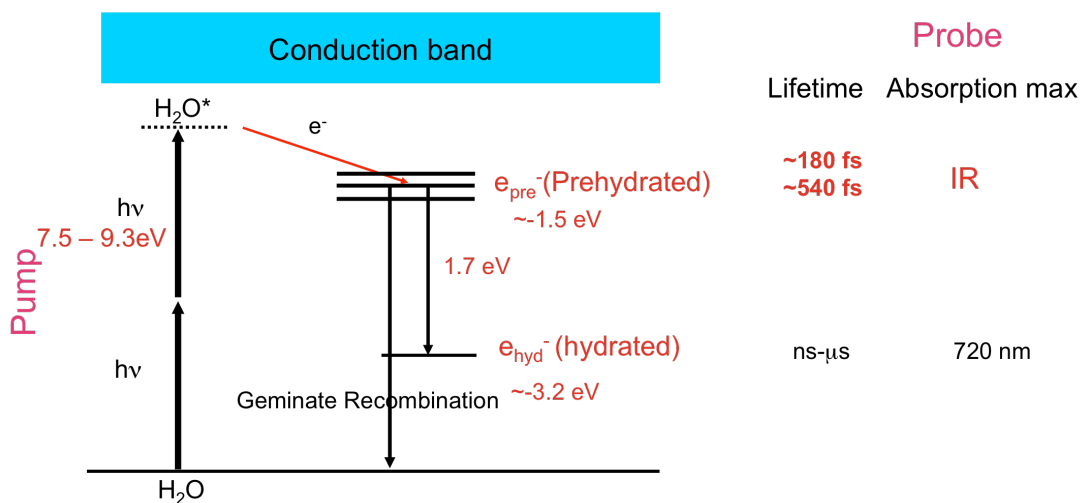
Figure 3.3 Generation of e_{pre}^- through two-photon UV excitation of H_2O
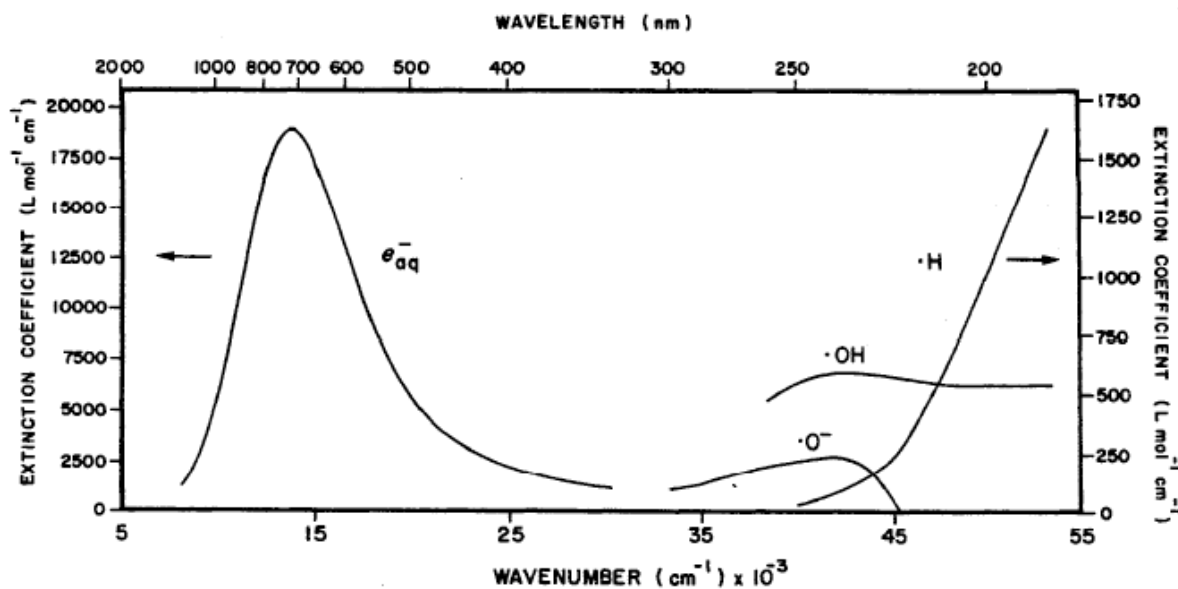
Figure 3.4 Absorption Spectrum of the radiolytic products of water. e_{aq}^- is the hydrated electron (e_{hyd}^-) [19]..

Using the femtosecond time-resolved pump-probe laser spectroscopy (fs-TRLS) technique, the transient absorption spectra are detected in real time, as shown in Figure 3.5.

In Figure 3.5, the x-axis represents the time delay between the pump and probe pulses in the units of picosecond (10^{-12} s). The y-axis is the absorbance of the hydrated electron to the probe wavelength, since the chosen probe wavelengths match the absorption band of the

33

hydrated electron. Before time delay zero, clearly no absorbance signal was present, indicating that before the excitation of water molecules by the pump pulse, the prehydrated electron and hydrated electron were not yet generated. At time delay zero, a fast rise in the electron absorptional signal is observed on the hundreds of femtosecond time scale. This time scale corresponds to the lifetime of the prehydrated electron, implying that the prehydrated electron is relaxing into the hydrated electron within the first several hundreds of femtoseconds, giving rise to the hydrated electron signal. Hence, the formation kinetics of the hydrated electron is equivalent to the decay kinetics of the prehydrated electron. In other words, the initial yield of the hydrated electron at around 1 ps is the same as the quantum yield of the prehydrated electron, that's why the initial yield of the hydrated electron is equivalent to the surviving yield of the prehydrated electron. This is an important notion since our theoretical calculations will be based on this point. Followed by the fast rise, a much slower decay was observed on the ns-μs time scale. The decay arises from the geminate recombination of e_{hyd}^- with cations (H_3O^+) and radicals ($^\bullet OH$ and $H^\bullet$) [19]. It is generally accepted that geminate recombination refers to the process where thermalized hydrated electron reforms water molecules upon reacting with cations (H_3O^+) and radicals present in solutions (mainly $^\bullet OH$ radical and solvated protons $H^\bullet$) [132].

By adding the electron scavenger potassium nitrate, one can clearly observe that as the scavenger concentration increases, the initial yield of the hydrated electron decreases accordingly. The decay kinetics of the hydrated electron remain relatively the same under different scavenger concentrations though. This phenomenon is clearly observed because the decaying traces are relatively parallel within the various concentrations, which reveals that the scavenging reaction is happening between the prehydrated electron and potassium nitrate rather than the hydrated electron and potassium nitrate for two reasons: first, the scavenging reactions take place within the first picosecond, corresponding to the lifetime of the prehydrated electron; second, if the reaction is occurring between the hydrated electron and
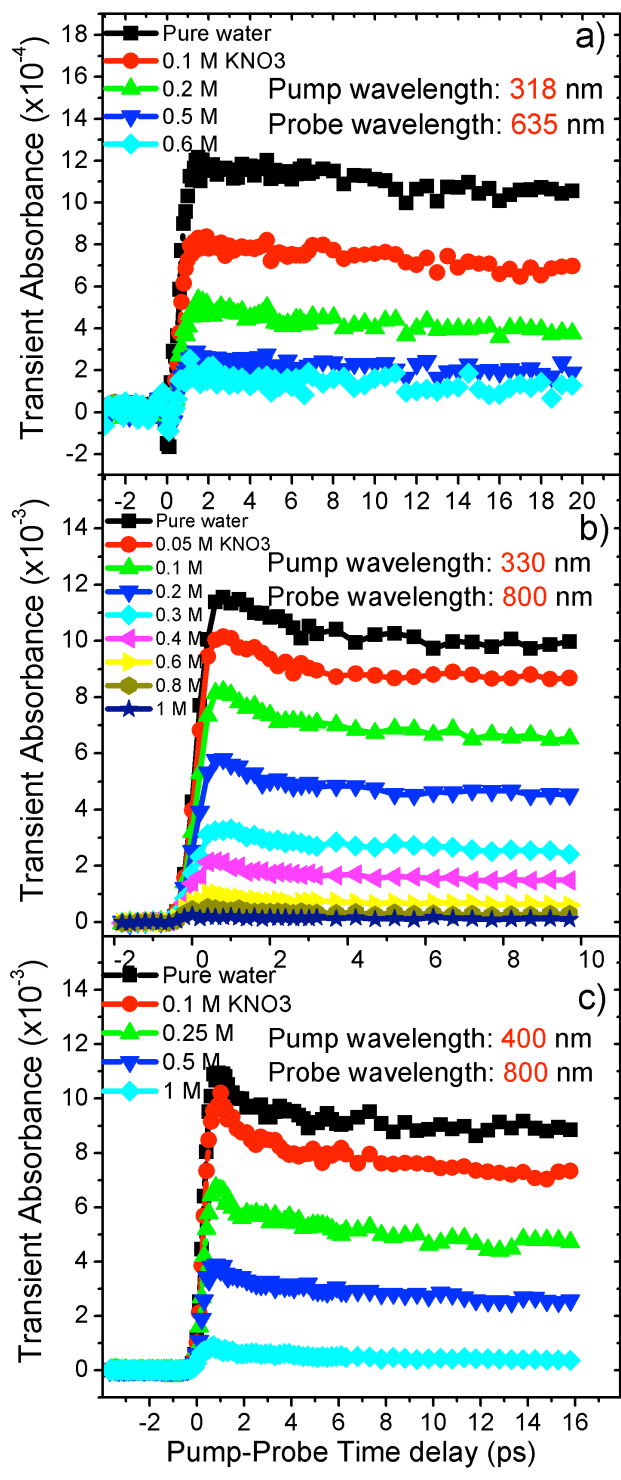
Figure 3.5 Transient absorption kinetic traces obtained from fs-TRLS technique.

the scavenger, one would observe a faster decay rate under higher scavenger concentration. However, faster decay kinetics were not found for higher KNO_3 concentrations.

As mentioned previously, potassium nitrate absorbs at pump wavelengths 318 and 330 nm. Therefore, under those laser conditions, KNO_3 absorption to the pump pulse has a minor attenuation of the pump intensity. This absorption loss will be taken into account in the later data analysis part.

3.4.2 The existence of coherence spike

In femtosecond pump-probe experiments, at time delay zero, a strong spike is often found. For example, under 7.8 eV and 7.5 eV excitation, at 2 M KNO_3 concentration when almost all precursor electrons are completely scavenged (except a small portion of the electrons that are beyond the reaction radius of KNO_3, hence the absorption signal is not zero), clearly at pump-probe time delay zero there still exists a narrow non-electron signal peak as illustrated in Figure 3.6.

This narrow peak is actually a non-resonant coherence spike, which is caused by the spatial and temporal overlap between pump and probe pulses at time delay zero. It has been observed universally in pump-probe experiments [101,106-109]. The existence of this coherence spike affects the accuracy of probed transient absorption curves. In order to eliminate this artificial effect, the spike signal obtained from 2 M KNO_3 solution is used as the artificial background to be subtracted from other transient absorption traces. The femtosecond time-resolved transient absorption traces with different scavenger concentration presented here under pump pulses of 318 nm, 330 nm and 400 nm, are all with coherence spikes removed.

However, the coherence spike can help to determine the time-delay zero. Time-delay zero is the point when pump and probe pulses overlap temporally at the exact moment, giving rise to the initiation of the experimental signal, as well as the coherence spike. Therefore, the coherence spike is centered at time delay zero point. By finding the peak of the coherence spike, the time-delay zero point can thus be determined. On the other hand, the coherence

spike reveals the response function of the laser pulse in the time domain from its FWHM. In our set-up, the response function was found to be 300 fs [101].
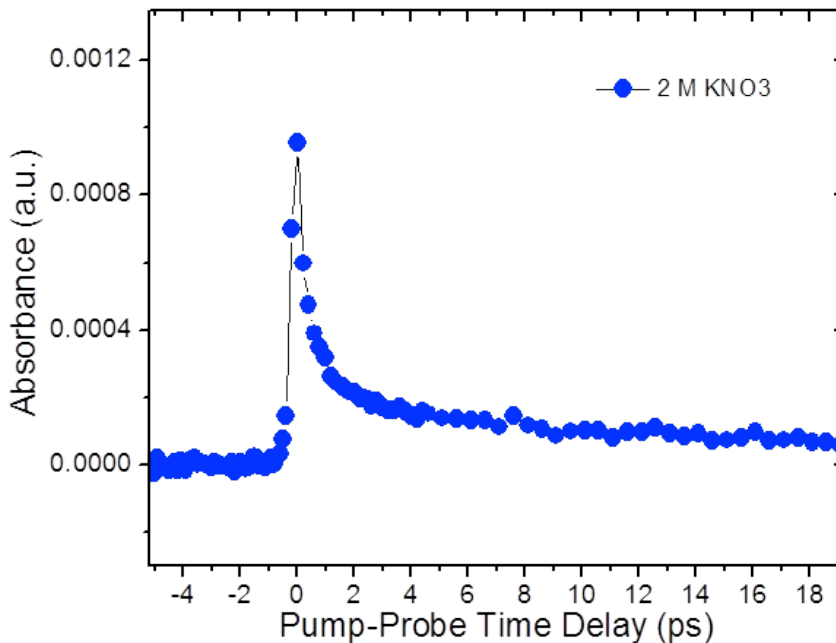
Figure 3.6 Coherence Spike at time delay zero as detected from a 2 M KNO_3 solution.

3.5 Results and Discussions

3.5.1 Scavenging Reactions

In order to derive the reaction rate constant of the scavenger and the prehydrated electron from the transient absorption spectra, the scavenging process is studied theoretically here. There are two important facts about the scavenging: first, the scavenging and hydration process of the prehydrated electron are in static competition, therefore competition kinetics can be applied; second, since the scavenger concentration in the scavenging process and the water concentration in the hydration process are both much greater than the concentration of the prehydrated electron ([S] >> [e_{pre}^-] and [M] >> [e_{pre}^-]), pseudo-first-order chemical kinetics can be used. The reaction equations are as illustrated below:

$$e_{pre}^- + M \xrightarrow{k_0} e_{hyd}^- \qquad (3.3)$$

$$e^-_{pre} + S \xrightarrow{k_s} S^{-1} \qquad\qquad \textbf{(3.4)}$$
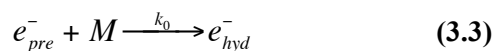
Where equation (3.3) shows the hydration process of the prehydrated electron, M is pure water. Equation (3.4) represents the scavenging process between the scavenger S and the prehydrated electron. Applying pseudo-first-order kinetics, [S] and [M] can be considered as static relative to the concentration of the prehydrated electron.

When there is no scavenger present, we only consider the hydration process, from equation (3.3):

$$\frac{Y}{Y_0} = e^{-k_0[M]t} = e^{-t/\tau_{pre}} \qquad\qquad \textbf{(3.5)}$$

Where Y is the yield of the prehydrated electron at time t, Y_0 is the total yield of the prehydrated electron and τ_{pre} is the intrinsic lifetime of the prehydrated electron.

When the scavenger S is added into the equation, one needs to consider both equation (3.3) and equation (3.4):

$$\frac{Y'}{Y_0} = e^{-(k_s[S]+k_0[M])t} = e^{-t/\tau} \qquad\qquad \textbf{(3.6)}$$

Where Y' is the yield of the prehydrated electron at time t in the presence of the scavenger S and τ is the lifetime of the prehydrated electron in the presence of the scavenger S.

From equation (3.5) and (3.6):

$$k_S[S] + \frac{1}{\tau_{pre}} = \frac{1}{\tau} \Rightarrow k_S[S] = \frac{1}{\tau} - \frac{1}{\tau_{pre}} \qquad \textbf{(3.7)}$$

Therefore, the percentage scavenging P_{sc} can be expressed as:

$$P_{sc} = \frac{Y-Y'}{Y} = 1 - \frac{e^{-t/\tau}}{e^{-t/\tau_{pre}}} = 1 - e^{-t(\frac{1}{\tau}-\frac{1}{\tau_{pre}})} \qquad \textbf{(3.8)}$$

Substitute equation (3.7) into equation (3.8):

$$P_{sc} = 1 - e^{-tk_S[S]} \qquad\qquad \textbf{(3.9)}$$

By definition, the percentage of survival is complement to the percentage of the scavenging, therefore:

$$P_{survival} = 1 - P_{SC} = e^{-tk_S[S]} \qquad (3.10)$$

At $t = \tau_{pre}$, we have:

$$P_{survival} = e^{-\tau_{pre}k_S[S]} \qquad (3.11)$$

The percentage of the prehydrated electron survived from scavenging is equivalent to the initial yield of the hydrated electron, therefore:

$$P_{survival} = Y_{int} = e^{-\tau_{pre}k_{pre}[S]} \qquad (3.12)$$

The plot of Y_{int} versus scavenger concentration [S] should follow an exponential relation with a parameter being the product of the lifetime of e_{pre}^- and the reaction rate constant we desired. Obtaining the initial yield of the e_{hyd}^- from transient absorption spectra under various scavenger concentrations and knowing the lifetime of the e_{pre}^- allow this rate constant to be determined.

3.5.2 Correction for KNO$_3$ absorption loss

Previously from the static absorption spectrum of KNO$_3$ we found that KNO$_3$ presents an absorption band around 300 nm. Therefore, the pump pulses with wavelengths of 318 and 330 nm, have their intensities attenuated by the KNO$_3$ absorption as they pass through KNO$_3$ solutions. Here we intend to develop a method to quantitatively correct for KNO$_3$ absorption loss.

Beer-Lambert law was stated previously. It describes the transmission of the light beam passing through the solution with the concentration of absorbing species being c, path length being l and ε being the extinction coefficient of the absorbing species at the wavelength of the light.

Furthermore, in two-photon excitation, the detected absorption signal intensity is quadratically dependent on the pump energy intensity. This relationship is verified

experimentally by measuring the absorption signal as a function of the power intensity of the pump pulse as illustrated in Figure 3.7.

Assume without KNO_3 absorption loss, the pump intensity is I_0 and detected signal intensity is A_0. With absorption by KNO_3, the pump intensity and signal intensity drop to I and A, then the following relation should hold.

$$\frac{I^2}{I_0^{\,2}} \propto \frac{A}{A_0} \qquad \textbf{(3.13)}$$

In addition, the ratio of initial yields (Y_{int}'/Y_{int}) with and without scavenger absorption loss should be proportional to the transmittance ($T=I/I_0$). Combining Beer-Lambert law with the rule of two-photon excitation, we have:

$$\frac{Y_{int}'}{Y_{int}} \propto \frac{A}{A_0} \propto T^2 = \frac{I^2}{I_0^2} = 10^{-2\varepsilon lc} \qquad \textbf{(3.14)}$$
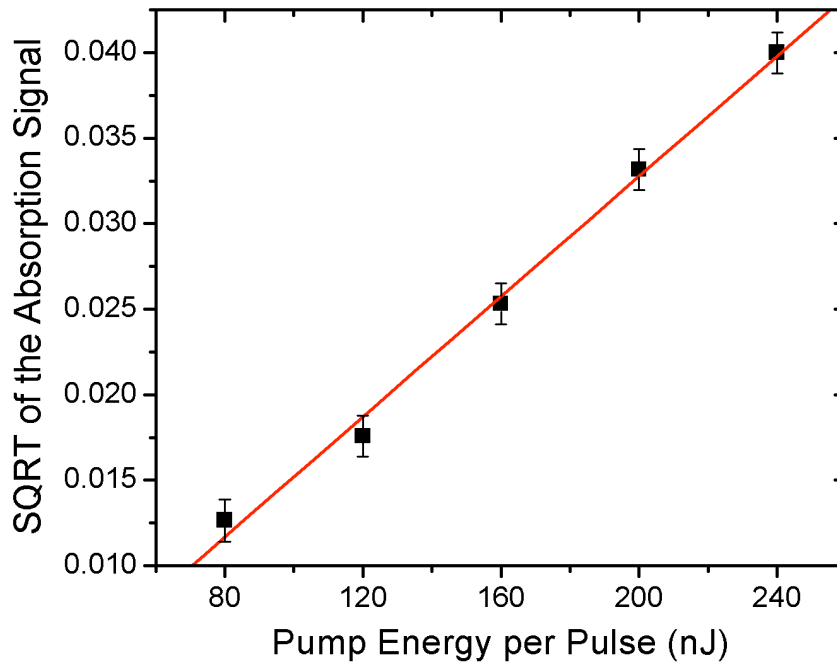

Figure 3.7 Square root of the absorption signal is proportional to the pump energy intensity

Therefore, the initial yield Y_{int} of the hydrated electron without attenuation of pump intensity by KNO_3 absorption can be expressed as:

$$Y_{int} = \frac{Y_{int}'}{T^2} \qquad \textbf{(3.15)}$$

Where Y_{int}' is the initial yield of the hydrated electron read directly from the real-time transient absorption spectra.

3.5.3 Reaction rate constants

Following equation (3.16), we corrected for KNO_3 absorption loss at 318 and 330 nm. Then the previous scavenging equation becomes:

$$Y_{int} = e^{-\tau_{pre}k_{pre}[S]} \qquad \textbf{(3.16)}$$

Plotting Y_{int} vs [S] for different pump wavelengths as illustrated in Figure 3.8. According to the scavenging equation 3.16, exponential fitting was performed on the data by using a least-square fitting program. Clearly, though pump and probe wavelengths vary, the exponential fittings of the data yielded similar results. Indeed, for other groups of data performed under similar experimental conditions, similar data fitting results were found. Due to space limitations, only 3 typical groups of data are shown here, they correspond to previous transient absorption spectra and they represent the experimental results under three different experimental conditions. The fitting parameter corresponds to the product of the lifetime of e_{pre}^- and the reaction rate constant we desired. The lifetimes of e_{pre}^- are 180 ± 30 and 545 ± 30 fs as determined previously [101]. Taking the average of all available data and taking the average lifetime of the prehydrated electron $\tau_{pre} = 360$ fs, the reaction rate constant of e_{pre}^- with KNO_3 is determined to be $k_{pre} = (0.75 \pm 0.5) \times 10^{13} \ \text{M}^{-1}\text{s}^{-1}$.
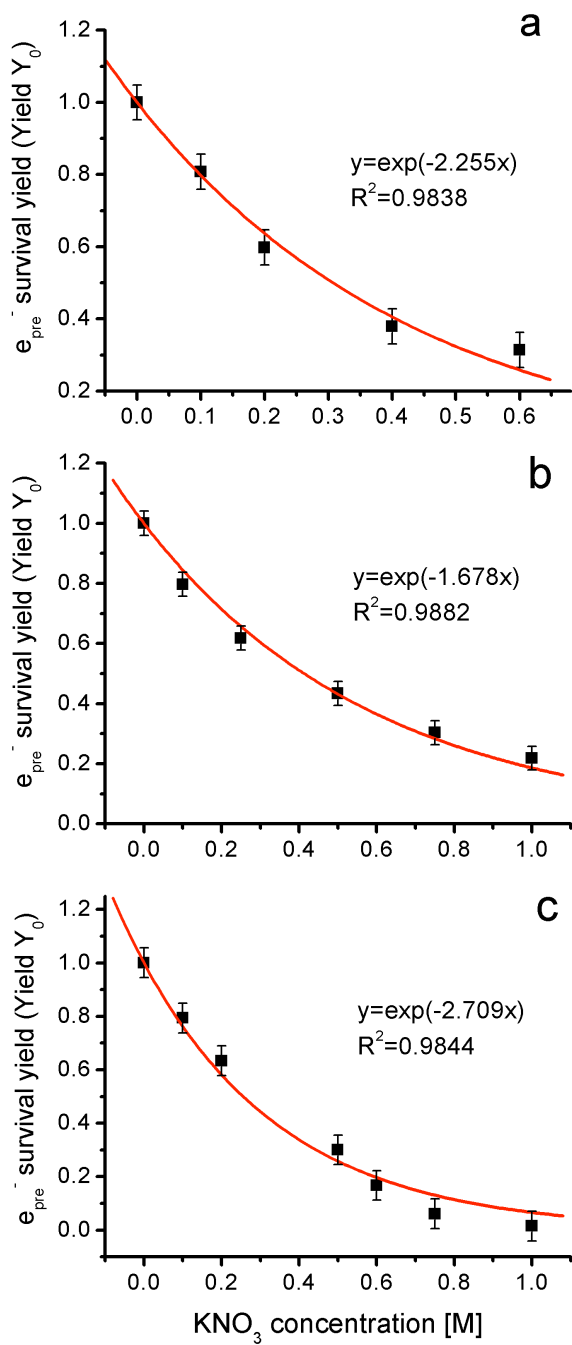
Figure 3.8 a: Y_{int} vs [S] for pump = 318 nm, probe = 635 nm; b: Y_{int} vs [S] for pump = 400 nm, probe = 800 nm; c: Y_{int} vs [S] for pump = 330 nm, probe = 800 nm; Error bars are derived from the least square fitting results.

The uncertainty in our experiments mainly arise from the set-up of our pump-probe experiments. For example, depending on the diameter of the pump beam, 1 M KNO_3 can either scavenge almost all of the prehydrated electron or leave about 10 % of the prehydrated electron depending on the photon density. Generally, when pump beam is unfocused (when the photon density is low), the former case takes place and when the pump beam is tight, more prehydrated electron can escape the scavenging.

It is interesting to compare our results with those of others. Back in the 1970s, the decreases in the initial yield of the hydrated electron in scavenging reactions were already observed using the picosecond pulse radiolysis equipment [91]. However, since the prehydrated electron was not directly observed back then, there lacked the correct mechanism to explain the observed decreases. Two categories of models have been proposed to explain the reduction in the initial yield of the hydrated electron. In one model, the existence of a presolvated state of the hydrated electron is proposed. The presolvated states of the hydrated electron can react with neighboring scavenger molecules before they become localized [91,133-138]. The other model is based on the encounter-pair model of Czapski and Peled [139], where they believed the free electron becomes localized first then reacts with the scavenger molecules. Other theories like the time-dependent reaction rate constant theory [140,141] and electron-tunneling model [142] both fall into the second category.

In 1987, Migus et al directly observed the precursor states of the hydrated electron [93], therefore, direct experimental observations supported the first model. Following the direct evidence of the prehydrated electron, researchers started to test the reaction of the hydrated electron scavengers with the precursor electrons of the hydrated electron. Some researchers have noticed not all the hydrated electron scavengers are prehydrated electron scavengers, but some of the scavenger molecules such as selenate ions (SeO_4^{2-}), nitrate ions (NO_3^-) and (Cd^+) are quite efficient at capturing the prehydrated electrons [95,96,143,144]. For example, from a "stochastic diffusion kinetic calculations", it was reported that 1 M NO_3^- scavenges ~90% of the electrons before hydration [95], which corresponds to a reaction rate constant of the nitrate ion with the prehydrated electron at around 0.6×10^{13} $M^{-1}s^{-1}$. Our results agree well with this value. *We have shown that at a 1 M concentration of nitrate ions, more than 90% of*

the prehydrated electrons are quenched. For concentrations as high as 2 M, KNO₃ can scavenge almost all of the prehydrated electrons available, leaving less than 5% remaining owing to the intermolecular distance of the prehydrated electron and the scavenger molecules. Moreover, previous studies on the scavenging of the prehydrated electron did not present the exact reaction rate constant of the nitrate ion and the prehydrated electron. Here, *for the first time, we report a quantitative analysis of the scavenging reaction, yielding a reaction rate constant of* $k_{pre} = (0.75 \pm 0.5) \times 10^{13}$ *M⁻¹s⁻¹*. Compare this reaction rate constant with that of the nitrate ion with the hydrated electron. The reported reaction rate constant of e_{hyd}^- and NO_3^- is $k = 9.7 \times 10^9$ M⁻¹s⁻¹ [19]. Therefore, *the reaction efficiency of* e_{pre}^- *and* NO_3^- *is two orders of magnitude larger than that of* e_{hyd}^- *and* NO_3^-, *which further confirms the high reactivity of* e_{pre}^-.

3.6 Concluding Remarks

This chapter presents direct observations of the ultrafast electron transfer reactions between the excited states of the hydrated electron (the prehydrated electrons) and the electron scavenger potassium nitrate. The experimental results were obtained from the femtosecond time-resolved pump-probe laser spectroscopy. The experimental results were analyzed using a derived scavenging theory and the quantitative scavenging efficiency was found to be $k_{pre} = (0.75 \pm 0.5) \times 10^{13}$ M⁻¹s⁻¹. This large reaction rate constant confirms the high reactivity of the prehydrated electron.

Chapter 4

Direct Observation of the Prehydrated Electron with OH radical Scavengers

4.1 Introduction

If one wishes to investigate the action of certain chemical species, this species will then inevitably be studied in control experiments, where either the species is eliminated from the experiment or the species is left alone in the experiments. In studies of the biological role of the prehydrated electron, besides the prehydrated electron, the other active radiolysis product of water is the hydroxyl radical, which has long been considered as the sole contributor to indirect radiation-induced DNA damage. Since we wish to compare the prehydrated electron-induced reductive DNA damage with the OH-radical-induced oxidative DNA damage, first, we have to apply the electron scavenger and leave the hydroxyl radical as the only active species in order to observe the effectiveness of the oxidative DNA damage. To aid such studies, we have already studied the efficiency of a compound that can eliminate the prehydrated electron. The scavenging efficiency of the electron scavenger potassium nitrate with the prehydrated electron is obtained. The second step would be to study the reductive DNA damage induced by the prehydrated electron in the absence of the oxidative DNA damage. Therefore, the prehydrated electron would need to be preserved as the only active species in water to facilitate controlled experiments. Hydroxyl radical scavengers can help to rule out the oxidative DNA damage by removing OH radicals. However, the reactions between the hydroxyl radicals and the prehydrated electron have never been studied. In order to achieve precisely controlled experiments, one has to investigate the possible reactions of the hydroxyl radical scavengers and the prehydrated electron, which is the main objective of this part of the project. Moreover, if such reactions exist, the reaction efficiency will be quantitatively determined.

The hydroxyl radical scavengers studied here are isopropanol and dimenthyl sulfoxide (DMSO). Both of them are well-known OH radical scavengers and are widely used in various biochemical experiments. The main advantage of applying DMSO as an OH radical

scavenger is that DMSO is generally less toxic to living biological systems. For example, in history, DMSO has been issued as a treatment drug for humans [145]. Generally a cellular environment can tolerate DMSO and isopropanol concentrations as high as 2 M.

4.2 Experimental Details

Similarly, the standard methodology of fs-TRLS was adopted here to obtain real-time observations of the scavenging reaction dynamics. The pump pulse was chosen at 330 to produce e_{pre}^- through the two-photon excitation process. The energy of pump pulse used in all experiments was between 80 nJ to 120 nJ. While the probe wavelength was chosen at 800 nm to probe the absorption signal of e_{hyd}^-.

Dimethyl sulfoxide (DMSO) and isopropanol from Caledon Labs was used as supplied. The PBS buffer used here contains 20 mM phosphate buffer (from NaH_2PO_4 and Na_2HPO_4) and 0.15 M NaCl. The pH value was adjusted to 7.40. Ultrapure water with a resistivity greater than 18 MΩ/cm was obtained from an ultrapure water system (Barnstead's Nanopure) with <1 ppb total organic content, which was used in all sample solutions. All sample solutions were held in a 5 mm quartz cuvette with a magnetic stirring bar to avoid any photoproduct accumulation. All static one-photon absorption spectra were taken using a UV/visible spectrophotometer (Beckman, Life Science). All experiments were performed at room temperature.

4.3 Static Absorption Spectra

As it was mentioned previously, our state-of-the-art femtosecond time-resolved pump-probe laser spectroscopy technique involves the photon excitation process to produce the prehydrated electron, therefore, the absorption of the excitation photons by the studied chemical compounds must first be considered. The static absorption spectra of isopropanol and DMSO are as follows:
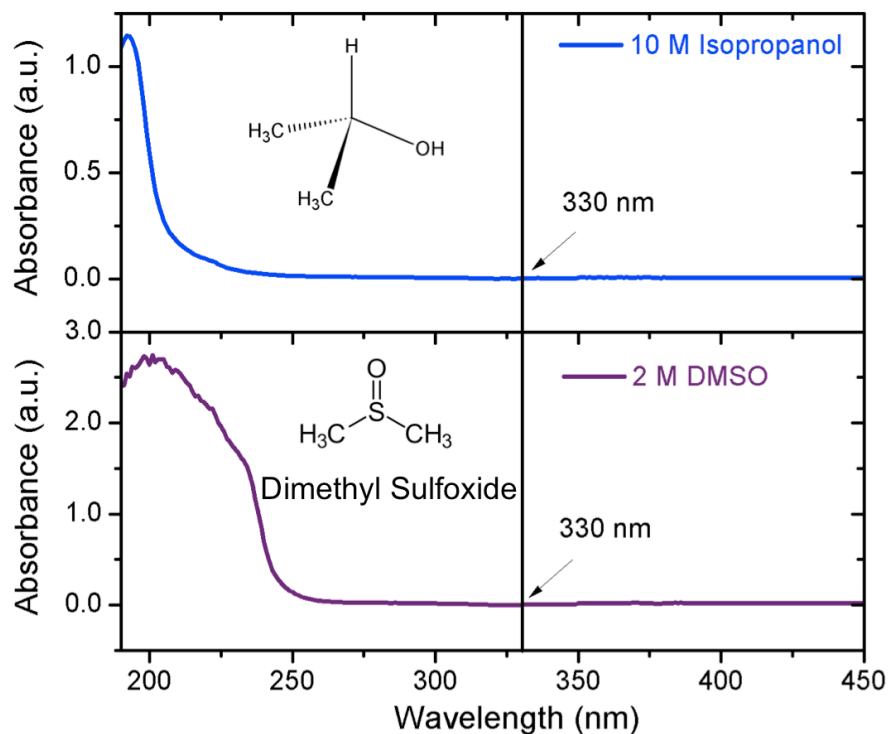
Figure 4.1 The static absorption spectra of isopropanol and DMSO.

Clearly, at the chosen wavelength of 330 nm, no absorption occurs. Hence no absorption loss is taken into account in the later data analysis part.

4.4 Transient Absorption Kinetic Traces

Transient absorption spectra of the hydroxyl radical scavengers were obtained using the fs-TRLS technique as introduced earlier. The pump pulse is chosen at 330 nm to excite water molecules through two-photon excitation with energy of 7.5 eV (2-photon), in order to generate the prehydrated electron. Once more, the probe pulse wavelength is selected at 800 nm to facilitate the second approach to study the prehydrated electron, which states that the final quantum yield of e_{pre}^- is essentially equivalent to the initial surviving yield of the hydrated electron.

4.4.1 Isopropanol

Transient absorption kinetic traces of isopropanol were detected in PBS buffer mixed the isopropanol solution. The solubility of isopropanol is excellent in PBS buffer because it is readily mixed with water at any concentration. PBS buffer is an important biological buffer that can maintain a stable environment for biological molecules or systems such as DNA molecules and cells. PBS buffer is non-toxic to cells, it can provide a stable environment with a pH value of 7.4. Moreover, the osmolarity and ionic concentration of the PBS buffer match those of the cells. Therefore, PBS buffer is widely used in biological experiments such as immunoassays, microbiological procedures and cell culture procedures, etc. We applied PBS buffer in DNA damaging experiments to stabilize the DNA molecules and minimize the effects of scavenging molecules on DNA. Hence, a direct observation of reaction dynamics in PBS buffer can directly be compared the results in biological experiments. The recipe for PBS buffer was introduced in the experimental details section. Isopropanol is miscible in PBS buffer solutions. The transient absorption spectra shown in Figure 4.2 were taken using the fs-TRLS technique, with isopropanol concentrations ranging from 0 (pure PBS buffer) to 3 M.

  The fast rise in the hydrated electron signal is observed at time-delay zero on a hundreds of femtosecond time scale, corresponding to the formation kinetics of the hydrated electron. These formation kinetics of the hydrated electron also correspond to the decay kinetics of the prehydrated electron. Following the fast rise in electron signal, the geminate recombination of the hydrated electron with cations and other radicals results in the slow decay of the hydrated electron. As isopropanol is added to the sample, the changes in the kinetic traces of the hydrated electron are observed. *Surprisingly, as the concentrations of isopropanol increase, the initial yield of the hydrated electron decrease accordingly*, but the decay trend of the hydrated electron remain the same for different concentrations of isopropanol. This finding directly proves that isopropanol scavenges the prehydrated electron though it is a well-acknowlegded OH radical scavenger. At the high isopropanol concentration of 2 M, about 25 % of the prehydrated electrons were eliminated by the isopropanol, implying that isopropanol is not only an OH radical scavenger, it is also an efficient electron scavenger.
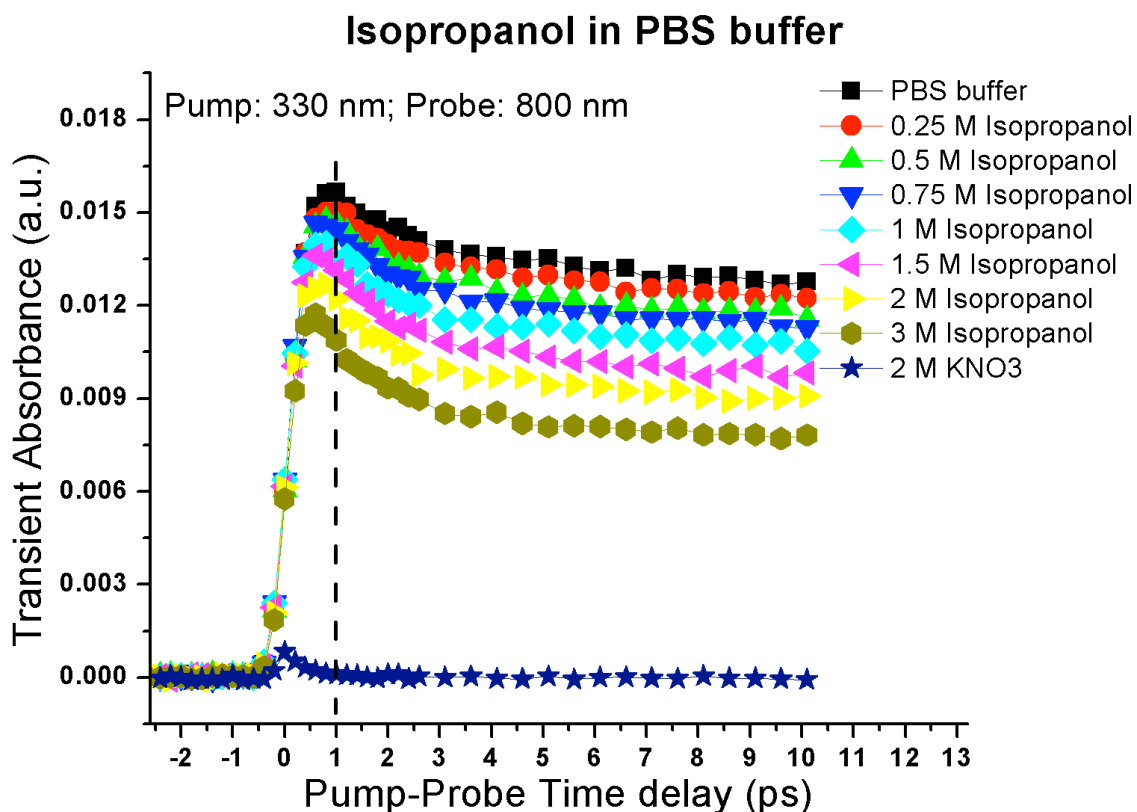
Figure 4.2 Transient absorption kinetic traces of isopropanol in PBS buffer solutions.

The coherence spike was detected by using a high concentration KNO_3 solution of 2 M and was included in the spectra. The intensity of this coherence spike is less than 10 % of that of the maximum absorbance signal. Therefore, the effect of the coherence spike on the transient absorption traces is negligible here.

4.4.2 DMSO

Dimethyl sulfoxide is commonly used as a biological reagent owing to its low toxicity to biological systems. It can be used as a cryoprotectant to prevent cell death from the freezing process, an inhibitor of DNA secondary structure formation in PCR (polymerase chain reaction), and a drug for treatment of interstitial cystitis [146,147]. In addition, it is a renowned $^{\bullet}OH$ scavenger. We utilize DMSO as an $^{\bullet}OH$ scavenger in our DNA damaging

experiments. Here we intend to investigate the possible reactions between DMSO and the prehydrated electron to precisely control the OH radical scavenging process.

Similar to the studies of isopropanol solutions, transient absorption spectra of DMSO were detected in PBS-buffer-mixed DMSO solution with the aim of directly comparing the DMSO scavenging efficiency of the prehydrated electron with that in the biological experiment. DMSO is miscible with water and various solvents. The spectra obtained here have concentrations of DMSO ranging from 0 (pure PBS buffer) to 3 M as illustrated in Figure 4.3.

The kinetic traces of the hydrated electrons were successfully detected in PBS buffer. In Figure 4.3, at time-delay zero, the hydrated electron signal arises from the decay kinetics of the prehydrated electron on hundreds of femtosecond time scale, corresponding to the formation kinetics of the hydrated electron. The geminate recombination of the hydrated electron with cations (H_3O^+) and other radicals ($^\bullet OH$) is reflected in the slow decay of the hydrated electron signal on a much longer time scale. When the concentration of DMSO increases, the initial yield of the hydrated electron decreases accordingly. Note that the decay trend of the hydrated electron remains relatively the same for the various DMSO concentrations, indicating the scavenging reaction is taking place between DMSO and the prehydrated electron rather than the hydrated electron. *Strikingly, the result shows that DMSO is an effective scavenger of the prehydrated electron though it is renowned OH radical scavenger. At DMSO concentration of 2 M, only 50~54 % of prehydrated electrons survived from DMSO scavenging, indicating that DMSO is a strong prehydrated electron scavenger.* This is more direct evidence proving that OH radical scavengers react with the prehydrated electron. Such observations have not been reported in the literature yet.
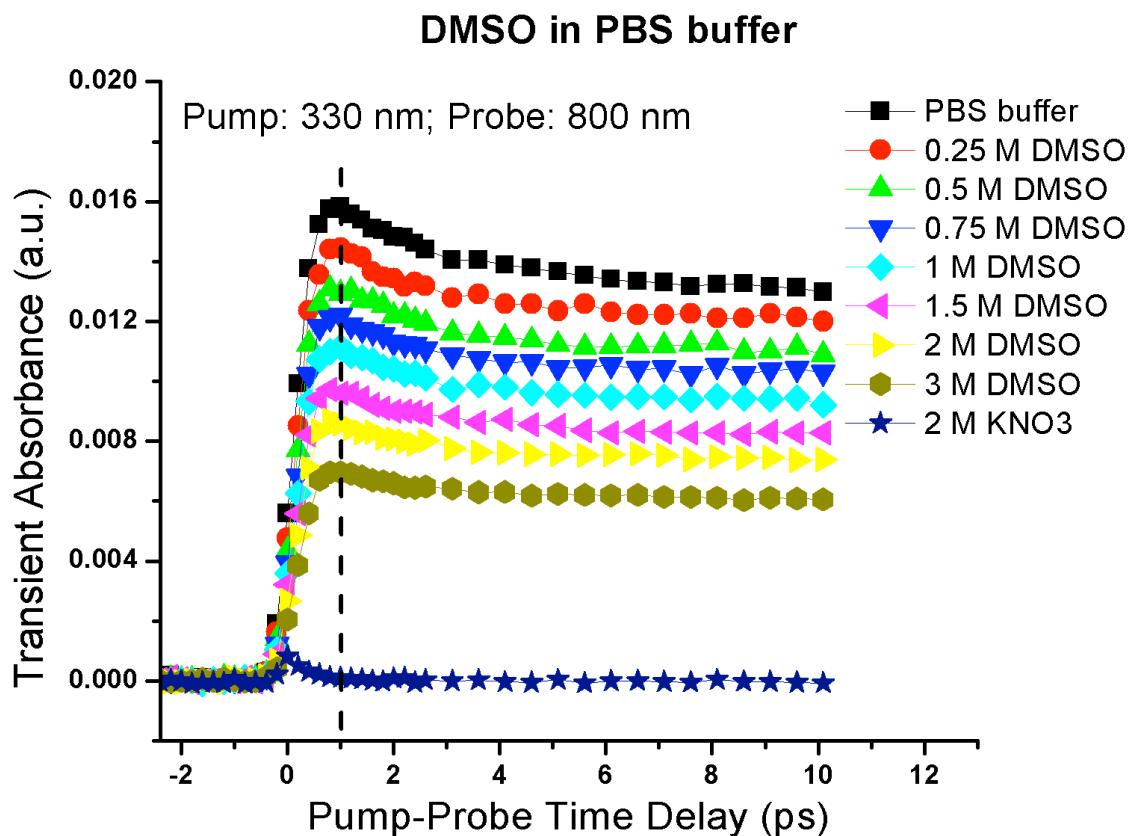
Figure 4.3 Transient absorption kinetic traces of DMSO in PBS buffer obtaind under pump pulse = 330 nm and probe pulse = 800 nm.

From the time-resolved absorption spectra of both isopropanol and DMSO solutions, the pump-probe coherence spike at time delay zero is less than 10 percent of the total signal intensity, as seen from the kinetic trace in high concentration of an electron scavenger KNO_3. Therefore, the effect of the coherence spike on the overall spectra is negligible.

4.5 Determination of Reaction Rate Constants

4.5.1 Isopropanol

The same methodology to calculate the reaction rate constant is adopted here. First, the surviving yield of e_{pre}^- is extracted from the transient absorption spectra of isopropanol at around 1 ps. According to the theory of scavenging derived in section 3.5.1, the surviving

yield of e_{pre}^- is an exponential function of the lifetime of e_{pre}^-, the scavenger concentration and the reaction rate constant we desire. Therefore, by fitting the surviving yield of e_{pre}^- vs isopropanol concentration using a built-in exponential function in a least-square fitting program, we can obtain the following results as illustrated in Figure 4.4.

From the figure, we extract the initial yield of the hydrated electron in the isopropanol-PBS mixed solutions and apply the same scavenging theory. Taking the lifetime of e_{pre}^- as 360 fs, the reaction rate constant of isopropanol with e_{pre}^- is determined to be $k = 3.3 \pm 0.5 \times 10^{11}$ $M^{-1}s^{-1}$ in PBS buffer.

Figure 4.4 Exponential data fitting different concentrations of isopropanol in PBS buffer solutions. Error bars are derived from the least square fitting results.

4.5.2 DMSO

The same methodology for calculating reaction rate constant is adopted here. First, the surviving yield of e_{pre}^- is extracted from the transient absorption spectra of DMSO from the initial yield of e_{hyd}^- at around 1 ps. According to the theory of scavenging, the surviving yield of e_{pre}^- is an exponential function of the lifetime of e_{pre}^-, the DMSO concentration and the

reaction rate constant we desire. Therefore, by fitting the surviving yield of e_{pre}^- vs DMSO concentration using a built-in exponential function in a least-square fitting program, we can obtain the following results as illustrated in Figure 4.5.

From the figure, we obtain the surviving yield of the prehydrated electron at each DMSO concentration and apply the scavenging theory. By taking the lifetime of e_{pre}^- as 360 fs, the reaction rate constant of DMSO with e_{pre}^- is determined to be $k = 8.7 \pm 0.5 \times 10^{11}$ $M^{-1}s^{-1}$ in PBS buffer.

DMSO in PBS Buffer
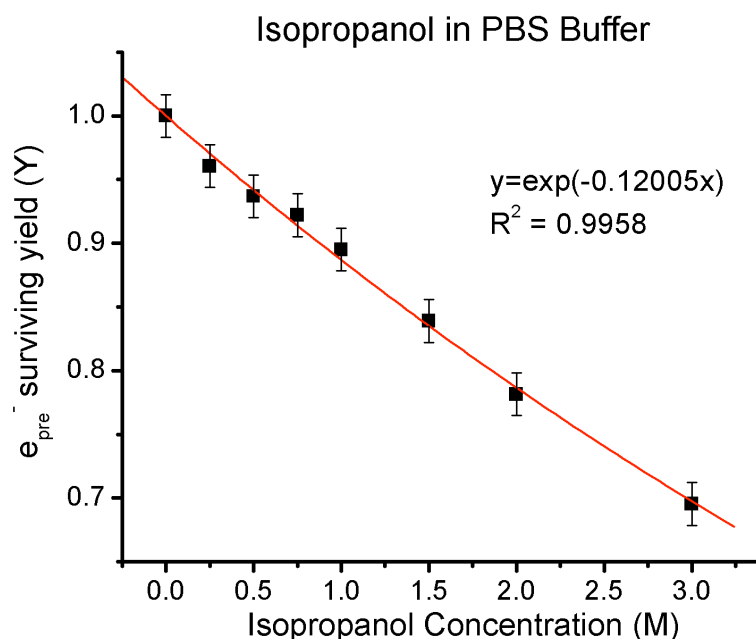

$y=\exp(-0.3135x)$
$R^2 = 0.9781$
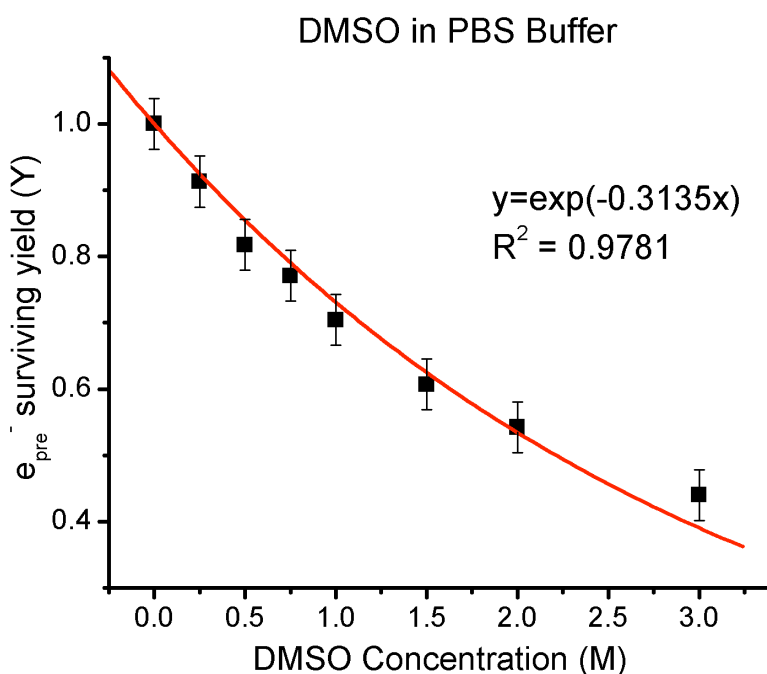
Figure 4.5 Exponential data fitting for DMSO in PBS buffer solutions. Error bars are derived from the least square fitting results.

It is interesting to compare our results of the electron scavenging ability with the OH radical scavenging ability of the OH radical scavengers. The reported OH radical scavenging reaction rate constants of isopropanol and dimethyl sulfoxide are: $k_{OH} = 2 \times 10^9$ $M^{-1}s^{-1}$ and 7×10^9 $M^{-1}s^{-1}$ [19]. *Clearly, the electron scavenging rate constants obtained here are two orders larger than the OH radical reaction rate constants. Moreover, these values are much larger than most reaction rate constants reported for the hydrated electron, as most reaction*

rate constants for the hydrated electron are on the order of magnitude of equal or less than $10^9 M^{-1}s^{-1}$ [19].

4.6 Concluding Remarks

This chapter presents the first direct observations of the ultrafast electron transfer reactions between e_{pre}^- and the OH scavengers isopropanol and DMSO. The experimental results were obtained using fs-TRLS and analyzed quantitatively, yielding large reaction rate constants compared to those of OH radicals with isopropanol and DMSO, which once more confirms the high reactivity of the prehydrated electron.

Chapter 5

Obtaining the Relative Yield Ratio of OH Radicals and the Prehydrated Electrons Using an $^\bullet$OH Scavenger

5.1 Introduction

Both the prehydrated electron and the hydroxyl radical are main radiolysis products of water under irradiation. While the hydroxyl radical was generally considered as the major contributor of radiation-induced DNA damage following radiotherapy treatment, we have recently shown that the reductive DNA damage induced by prehydrated electrons could be even more effective than the oxidative DNA damage caused by OH radicals [12,24]. In order to compare the efficiencies of $^\bullet$OH and the e_{pre}^- at inducing biological damage, the relative yield ratio of both species ($r = [^\bullet OH]/[e_{pre}^-]$) is an important quantity to analyze and facilitate the prediction of the biological efficiency of $^\bullet$OH and e_{pre}^-.

Previous studies on the relative yield ratio of $^\bullet$OH and the e_{hyd}^- have shown that as the radiation energy decreases, $r = [^\bullet OH]/[e_{hyd}^-]$ increases [148,149]. For ionizing x-ray radiation, the accepted ratio of yields is around 1:1 at 10^{-6} s following the radiation. As the energy lowers, the ratio increases. For instance, for two-photon UV radiation at 200 nm, r is reported to be 1.1±0.3 [148] and for 266 nm, the reported ratio is 1.7±0.9 [148] or 1.9 [149]. When the radiation wavelength increases to 299 nm, the ratio r was reported to be 3.3±1.0 or even > 8 in the literature [148]. These observations can be explained by the fact that the lower the excitation energy is, the more water molecules go through the dissociation channel to generate $^\bullet$OH rather than the ionization process which produces more electrons than $^\bullet$OH.

The state-of-the-art femtosecond time-resolved pump-probe laser spectroscopy is a fantastic tool to study ultrafast reactions of radicals and electrons at the femtosecond level. It can provide direct observations of the radiolytic species of water molecules following two-photon UV excitation. As we discussed previously, the direct observation of the prehydrated electron was feasible using two approaches: detecting the prehydrated electron in the infrared region; or probe the hydrated electron in the visible region, whose formation kinetics

correspond the decay kinetics of the prehydrated electron. However, the direct spectroscopic observation of $\cdot$OH radicals is quite difficult due to the spectroscopic overlap of the $\cdot$OH radical absorption band at 230 nm with other species (for example, the hydrated electron) [150]. Therefore, in order to observe the reaction dynamics of OH radicals and derive the quantum yield ratio r, another scavenger of $\cdot$OH is necessary to produce a scavenging product with visible absorption band.

Thiocyanate ion (SCN$^-$) is an effective OH radical scavenger that can react with an OH radical rapidly following two steps:

$$(1) SCN^- + \,^\cdot OH \rightarrow SCN^\cdot + OH^-$$

$$(2) SCN^\cdot + SCN^- \rightarrow (SCN)_2^{\cdot -}$$
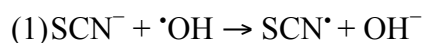
The rate constant of reaction (1) was reported to be $k = 2.8 \times 10^{10}\,M^{-1}s^{-1}$ or a combined reaction rate constant of the above scavenging reaction was reported to be $k = 1.1 \times 10^{11}\,M^{-1}s^{-1}$ [19]. The absorption maxima of the product was at around 475 – 480 nm, and it was first assigned to SCN$^\cdot$ [151]. However, it was pointed out later that it is $(SCN)_2^{\cdot -}$ from reaction (2) that contributes to the absorption band around 475 nm with the extinction coefficient being $\varepsilon = 7100\,M^{-1}cm^{-1}$ and at around 480 nm with the extinction coefficient being $\varepsilon = 7600\,M^{-1}cm^{-1}$ [152,153].

There have been a number of studies utilizing SCN$^-$ to quantify the amount of OH radical in aqueous solution, as well as applying SCN$^-$ as an OH radical scavenger to obtain the reaction rate constant of $\cdot$OH with other substances through competition kinetics. For example, Zeller et al used thiocyanate ion to determine the quantum yield of OH radical under the photolysis of nitrate and nitrite ions [154]. Here we intend to detect the thiocyanate dimer radical $(SCN)_2^{\cdot -}$, from which the reaction dynamics of $\cdot$OH can be observed. Moreover, the quantum yield ratio of $\cdot$OH and the e_{pre}^- ($r=[\cdot OH]/[e_{pre}^-]$) can be deduced to aid the comparison of oxidative DNA damage caused by $\cdot$OH and reductive DNA damage induced by the e_{pre}^-.

5.2 Experimental Details

Similarly, the standard methodology of fs-TRLS was adopted here to obtain real time observations of the scavenging reaction dynamics. The pump pulse was chosen at 330 nm and 266 nm to produce the e_{pre}^- through two-photon excitation process. The energy of the pump pulse used in all experiments was between 80 nJ to 240 nJ. While the probe wavelength was chosen at 480 nm to probe the absorption signal of $(SCN)_2^{\bullet-}$ and 800 nm to probe the absorption signal of the e_{hyd}^-.

Potassium thiocyanate from Sigma Aldrich was used as supplied. Ultrapure water with a resistivity greater than 18 MΩ/cm was obtained from an ultrapure water system (Barnstead's Nanopure) with <1 ppb total organic content, which was used in all sample solutions. The PBS buffer used here contains 20 mM phosphate buffer (from NaH_2PO_4 and Na_2HPO_4) and 0.15 M NaCl. All sample solutions were held in a 5 mm quartz cuvette with a magnetic stirring bar to avoid any photoproduct accumulation. All static one-photon absorption spectra were taken using a UV/visible spectrophotometer (Beckman, Life Science). All experiments were performed at room temperature.
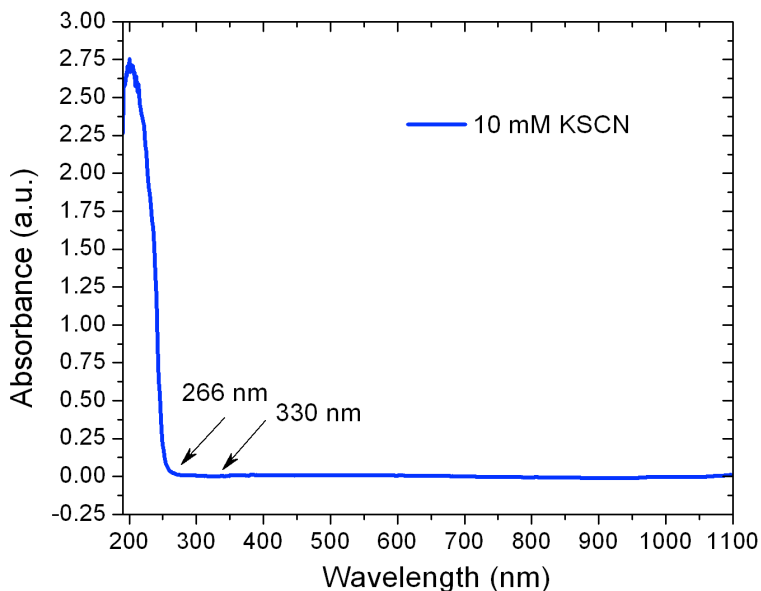

Figure 5.1 Static absorption spectrum of 10 mM KSCN solution.

5.3 Static Absorption

The static absorption spectrum of potassium thiocyanate (KSCN) is taken to assist the selection of pump and probe wavelength. As shown in Figure 5.1, potassium thiocyanate does not absorb in the near ultraviolet, visible and near infrared region. Therefore, at our pump wavelength 330 nm and 266 nm, no attenuation of the pump pulse by KSCN should occur.

5.4 Transient Absorption Kinetic Traces

Transient absorption kinetic traces of potassium thiocyanate were obtained using the fs-TRLS technique as introduced earlier. In the biological experiment to assess the effectiveness of the prehydrated electron, we have applied PBS buffer to to stabilize the DNA molecules and minimize the effects of scavenging molecules on DNA. Therefore, all KSCN solutions are prepared in PBS buffer, in order to compare the results with those in the biological experiments that applied PBS buffer. The pump pulse is chosen at 330 nm to excite water molecules through two-photon excitation with energy of 7.5 eV, to generate $^{\bullet}$OH radicals. The probe pulse wavelength is selected at 480 nm, to facilitate the detection of $(SCN)_2^{\bullet-}$, which has the maximum absorption band between 475 – 480 nm [151].

As observed from Figure 5.2, increasing the concentration of KSCN solution induces a larger absorption signal at 480 nm. Moreover, the decay trend of KSCN solutions appears to be different than the decay trend in pure water sample. These observations lead to the speculation that the increased absorption signal comes from $(SCN)_2^{\bullet-}$. In addition, if we zoom in Figure 5.2 to a shorter time scale (< 20 ps) then we can actually observe that clearly at the short time scale, when the KSCN concentration becomes larger, the initial yields of the detected products increases correspondingly, as shown in Figure 5.3. Therefore, the absorption signal increases consist of two parts: the increases in the initial yields of the product on the ultrafast time scale (~ 1 ps) and the increases of the absorption product on a much longer time scale (~ several nanoseconds). These two types of increases can be attributed to two states of $^{\bullet}$OH radicals: an excited "hot" OH radical state which occurs on the ultrafast time scale with short lifetime and the "cold" ground-state OH radicals with much

longer lifetime [24]. The scavenging product $(SCN)_2^{\bullet-}$ was observed previously on nanosecond even microsecond time scale [150]. One can infer $(SCN)_2^{\bullet-}$ has a relative long lifetime possibly extending a few microseconds. Therefore, on the nanosecond time scale, the detected signal comes from two parts: the first part comes from the accumulated $(SCN)_2^{\bullet-}$ products from the reaction of KSCN with "hot" OH radicals; Moreover, in the low concentration KSCN solutions present here, some of the "hot" OH radicals can escape the scavenging reactions, relaxing into the "cold" OH radical states. Therefore, the second part of the signal is the $(SCN)_2^{\bullet-}$ product produced from the reaction of KSCN with "cold" OH radicals. The latter leads to the rise of the signal on the nanosecond time scale, which agrees with the lifetime of the "cold" OH radicals.
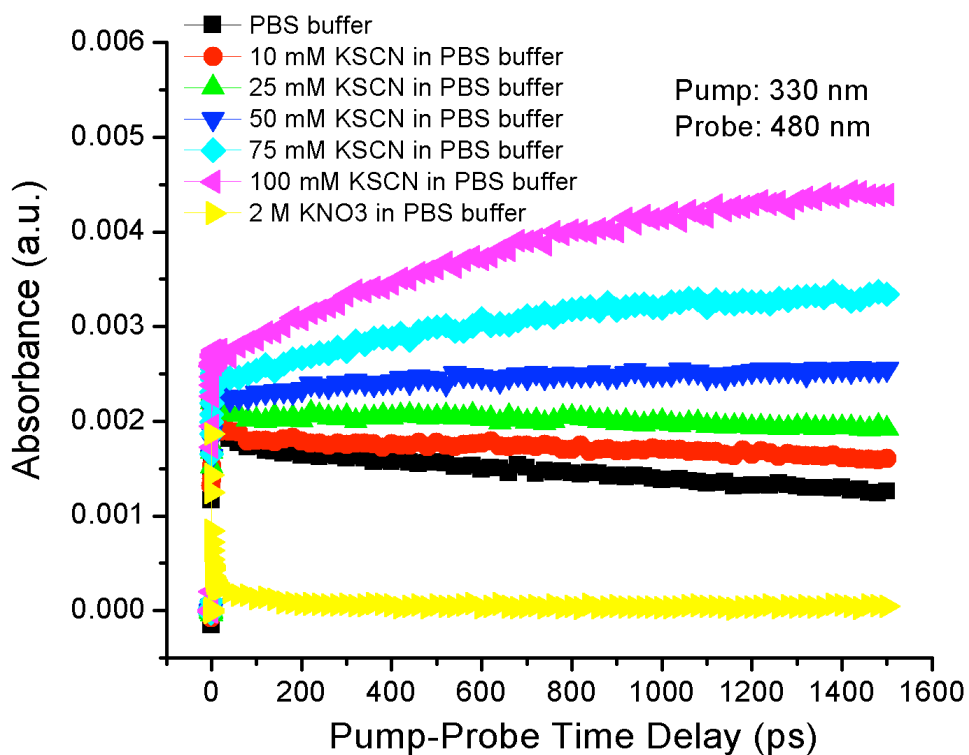

Figure 5.2 Transient absorption spectra of KSCN in PBS buffer solutions at a long time scale (~ 1500 ps). Pump wavelength = 330 nm, probe wavelength = 480 nm.

However, we have to be careful in making such conclusions since at 480 nm, clearly the hydrated electron absorbs the light as well. Therefore, in order to rule out the possibility that the increasing signal is an electron signal, two approaches were performed. For the first approach we applied an additional $^{\bullet}$OH radical scavenger into KSCN solution, if the increasing signal is quenched in the $^{\bullet}$OH scavenger solution, then the signal should be the same with that in pure water. The other method to distinguish the real $(SCN)_2^{\bullet-}$ signal from the electron signal is to detect the hydrated electron signal directly around its maximum absorption in KSCN solutions, for example, in our case we choose 800 nm. If KSCN solutions do not produce extra electron signal under 800 nm detection, than the absorption signal detected under 480 nm should belong to $(SCN)_2^{\bullet-}$.
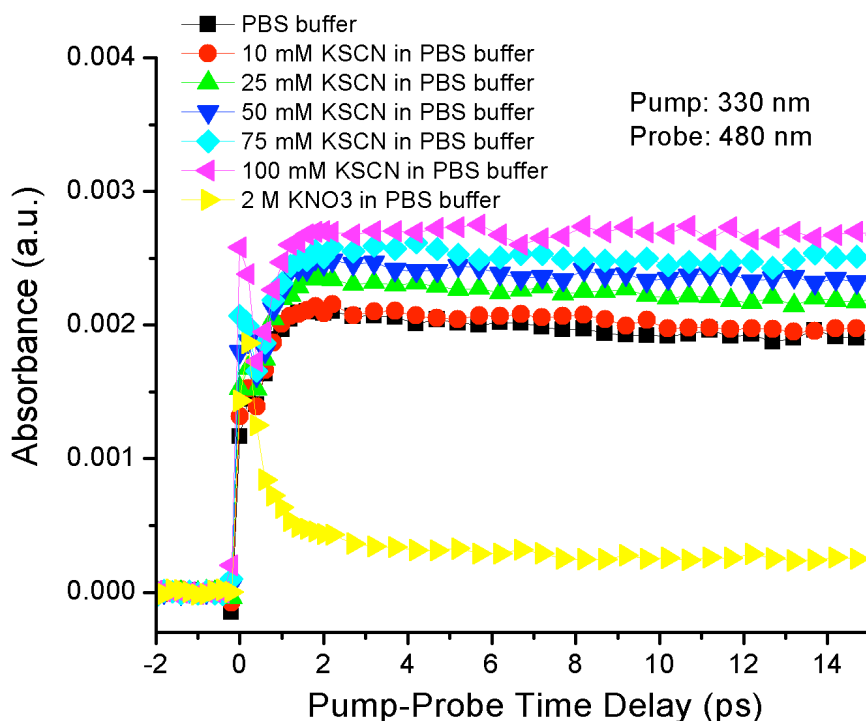
Figure 5.3 Transient absorption spectra of KSCN in PBS buffer solutions at a short time scale (~15 ps). Pump wavelength = 330 nm, probe wavelength = 480 nm.

First, isopropanol as an $^{\bullet}$OH radical scavenger is applied in KSCN solutions. As one can observe from Figure 5.4, in the presence of 2 M isopropanol, the absorption signal decreased
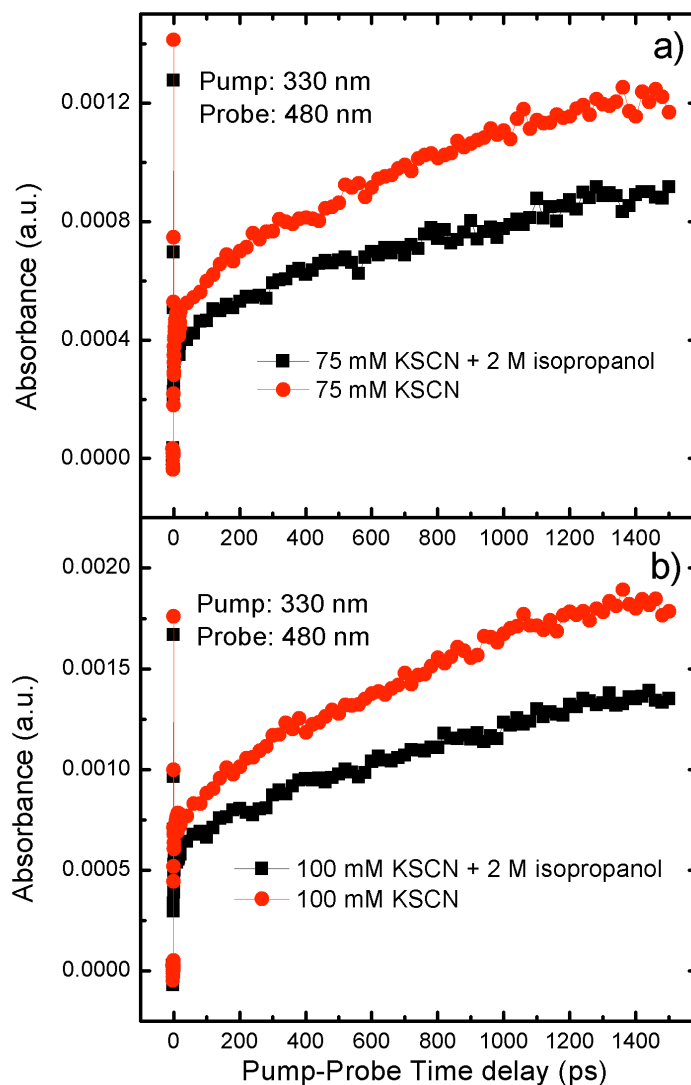
Figure 5.4 Transient absorption spectra of KSCN with isopropanol in PBS buffer solutions. Pump wavelength = 330 nm; Probe wavelength = 480 nm.

significantly in KSCN solutions. This indicates that 2 M isopropanol is able to quench the previous increasing signal in KSCN solutions. Therefore, the increasing signal in KSCN solutions involves OH radicals. However, even though isopropanol was applied at a high concentration, it was not able to quench the increasing signal completely. This is due to the fact that the two OH radical scavengers are in competition with each other. As it was pointed

out in the literature, KSCN is a strong OH radical scavenger, it scavenges OH radicals according to the combined reaction:

$$2SCN^- + {}^{\bullet}OH \rightarrow (SCN)_2^{\bullet-} + OH^-$$
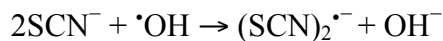
whose rate constant is reported to be $k = 1.1 \times 10^{10}$ $M^{-1}s^{-1}$ [19,155]. This rate constant is an order larger than that of isopropanol with OH radicals: $k_{isopropanol} = 2 \times 10^9$ $M^{-1}s^{-1}$ [19]. Therefore, KSCN competes aggressively with 2 M isopropanol in the above experiments. As a result, 2 M isopropanol is not strong enough to quench all of the OH radicals before KSCN reacts with them. On the other hand, we have discussed that ${}^{\bullet}OH$ radical scavenger isopropanol is also an electron scavenger. One may argue that when isopropanol was applied in KSCN solutions, it quenched the electron signal as well. However, we have already considered such scavenging effect by subtracting the PBS buffer absorption trace and PBS buffer + 2 M isopropanol from the original 75/100 mM KSCN solutions in PBS buffer and 75/100 mM KSCN solutions with 2 M isopropanol in PBS buffer absorption traces, respectively, as shown in Figure 5.4. Therefore, the influence of electron signal on these $(SCN)_2^{\bullet-}$ absorption signal have been eliminated. Hence, the change in electron signal by isopropanol is irrelevant after eliminating electron signal.

The second approach to distinguish the detected species from the electron signal intends to probe the electron signal directly. Therefore, the probe wavelength is selected at 800 nm, the pump pulse at 266 nm is used to produce prehydrated electrons and ${}^{\bullet}OH$ radicals. The transient absorption spectra are obtained in Figure 5.5.

Figure 5.5 clearly shows that the KSCN solutions do not produce prehydrated electrons under UV irradiation. Otherwise, as KSCN concentration increases, the absorption signal should increase correspondingly. This observation is further evidence that the signal detected in our experiments under 480 nm was in fact the $(SCN)_2^{\bullet-}$ signal.
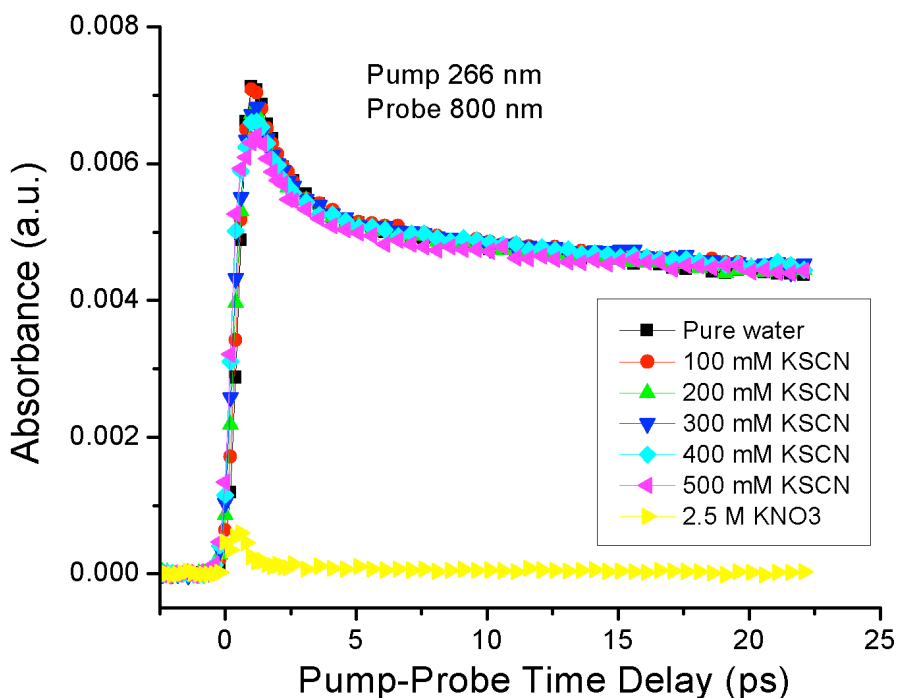
Figure 5.5 Time-resolved transient absorption spectra of KSCN solutions detected using pump wavelength = 266 nm, probe wavelength = 800 nm.

Furthermore, high concentrations of KSCN solutions show the same signal increases as demonstrated in Figure 5.6.

Interestingly, at concentrations above 2 M, KSCN absorption traces under 480 nm overlap with each other. This observation demonstrates that at concentrations higher than 2 M, the absorption signal of the reaction product between KSCN and $^\bullet$OH radical is saturated. In contrast to the low concentration KSCN solutions, under the high KSCN concentration ($\geq$ 2 M), the "hot" OH radicals should be much less likely to escape the scavenging reaction. Similar trend was observed in the scavenging reaction of the prehydrated electron with KNO_3, where the surviving yield of the prehydrated electron decreased significantly with increasing KNO_3 concentrations. Eventually under 1 M KNO_3, more than 90 % of the prehydrated electron was quenched. Hence, under 2 M KSCN concentration, the "hot" OH radicals probably were almost completely quenched by the SCN^- ions before they relax into

the "cold" OH radical states. This also explains why under higher concentration, no rises in the absorption signal were observed on the nanosecond timescale. In contrast, the slow decay was observed in the high concentration KSCN solutions, which might be attributed to the recombination of the $(SCN)_2^{\bullet-}$ with other ions or radicals in the solution. Therefore, the saturated absorption intensity of $(SCN)_2^{\bullet-}$ under 480 nm should be approximately equal to the amount of "hot" OH radicals produced from water radiolysis. Using the saturated absorption intensity, one can obtain the relative yield ratio of "hot" $^\bullet$OH radicals compared to the hydrated electrons, as shown in the following results and discussion section.

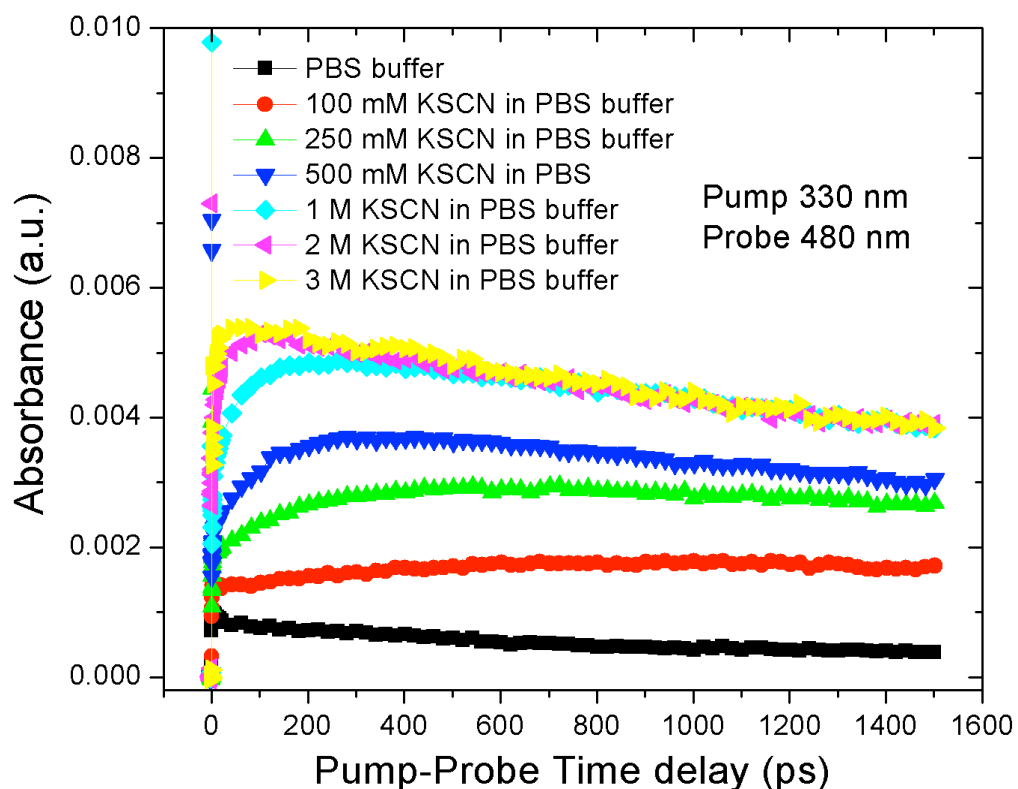**Figure 5.6** Time-resolved transient absorption spectra of relatively high concentrations of KSCN solutions in PBS buffer detected using pump wavelength = 330 nm, probe wavelength = 480 nm.

In summary, the observed increasing signal is attributed to the formation of $(SCN)_2^{\bullet-}$ and not the electron signal because: first the detected species have strong absorption at 480 nm,

which agrees well with the absorption spectra of $(SCN)_2^{\bullet-}$; Second, to rule out that the signal increases are caused by the electron signal, applying another OH radical scavenger isopropanol at suitable concentration is able to reduce the increased signal, which means the formation of the detected transient species involve OH radicals; Third, by changing the probe wavelength to the electron absorption wavelength 800 nm, we show that KSCN solutions do not produce extra electrons under irradiation. Moreover, the observed increase in signal rises rapidly on picosecond time scale. This supports the prediction of the existence of "hot" OH radicals [24].

5.5 Results and discussions

From the high concentration data, one can see that at concentration higher than 2 M, the absorption signal of $(SCN)_2^{\bullet-}$ is saturated in KSCN solutions. According to the discussions in section 5.4, the amount of $(SCN)_2^{\bullet-}$ detected should be equal to the amount of "hot" OH radicals produced in the sample. Hence, the relative yield ratio of "hot" OH radical and the hydrated electron can be derived by knowing the absorption signal intensities of both $(SCN)_2^{\bullet-}$ and the hydrated electron, as well as the extinction coefficients of both species at the probe wavelength 480 nm. The following relation can be used

$$\frac{A_{(SCN)2\bullet-}}{A_{ehyd}} \propto \frac{\varepsilon_{(SCN)2\bullet-}}{\varepsilon_{ehyd}} \bullet \frac{[{}^{\bullet}OH_{hot}]}{[e_{ehyd}]}$$

Where $A_{(SCN)2\bullet-}$ is the absorption intensity of the observe $(SCN)_2^{\bullet-}$ signal, A_{ehyd} is the observed hydrated electron absorption intensity. $\varepsilon_{(SCN)2\bullet-}$ and ε_{ehyd} are the extinction coefficients of $(SCN)_2^{\bullet-}$ and the hydrated electron, respectively. Therefore the relative yield ratio r= $[{}^{\bullet}OH_{hot}]/e_{hyd}^-$ can be obtained by knowing the above parameters.

From the literature, the reported extinction coefficient for $(SCN)_2^{\bullet-}$ at 480 nm is $\varepsilon_{(SCN)2\bullet-}$ = 7600 $M^{-1}cm^{-1}$ [153]. On the other hand, the absorption spectrum of the e_{hyd}^- has been known for decades and the reported extinction coefficient for the e_{hyd}^- at 480 nm is ε_{ehyd}= 4750 $M^{-1}cm^{-1}$ [19,156]. The absorption intensities of both species can be directly read off from the transient absorption spectra obtained using fs-TRLS. Before getting the absorption intensity of $(SCN)_2^{\bullet-}$, the electron signal must be subtracted from the transient absorption traces of

KSCN solutions. After the subtraction, the transient absorption traces of KSCN should represent solely the dynamics of $(SCN)_2^{\bullet-}$, as shown in:
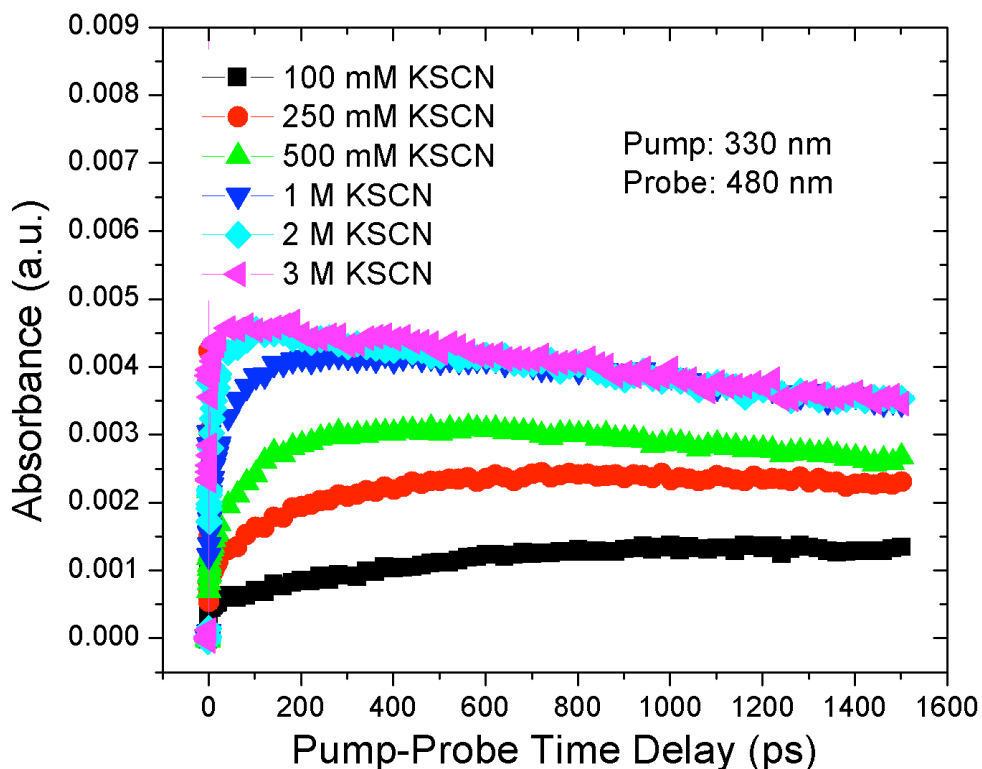
Figure 5.7 Time-resolved transient absorption spectra of relatively high concentrations of KSCN in PBS buffer solutions after subtracting the electron signal.

After comparing the absorption intensity of $(SCN)_2^{\bullet-}$ and the e_{hyd}^- at ~1 ns, we obtain the relative yield ratio of "hot" $^\bullet OH$ radicals and e_{hyd}^- under 330 nm irradiation is:

$$\frac{[^\bullet OH_{hot}]}{[e_{hyd}]} \propto \frac{A_{(SCN)2\bullet-}}{A_{ehyd}} \bullet \frac{\varepsilon_{ehyd}}{\varepsilon_{(SCN)2\bullet-}} = \frac{3.816 \times 10^{-3}}{4.347 \times 10^{-4}} \bullet \frac{4750}{7600} = 5.5 \pm 0.8$$

The initial yield of the prehydrated electron produced within 10^{-14} s is about twice as much as that of the hydrated electron around 10^{-6} s [19]. Moreover, about 64% of e_{pre}^- (~10^{-14} s) relax into e_{hyd}^- (~ 10^{-12} s) [97] and the yield of e_{hyd}^- decreases by 10% at 10^{-9} s compared to

that at 10^{-12} s [157]. Therefore, at around 10^{-9} s, the yield of e_{hyd}^- is at least half of the initial yield of e_{pre}^-. Hence, if we take the upper limit that e_{pre}^- (10^{-14} s)/e_{hyd}^-(10^{-9} s)=2:1 and neglect the recombination of $(SCN)_2^{\bullet-}$ with other ions, then, the relative yield ratio r= [$^{\bullet}OH$]/[e_{pre}^-] is at least 2.8 ± 0.4, where the uncertainty in this value mainly comes from the approximations we made for e_{pre}^- (10^{-14} s)/e_{hyd}^-(10^{-9} s) ratio, and the laser beam condition as discussed in Chapter 3, section 3.5.3.

Comparing our results with those reported in the literature, it was reported that when radiation wavelength increases to 299 nm, the ratio r becomes 3.3 ± 1.0 or even > 8 [148]. As the wavelength extends to 330 nm, the relative yield ratio r will increase accordingly as explained previously. Therefore, for those reported values, if the wavelength is extended to 330 nm, we find that our results would be close to the first value obtained by Elles et al, whereas Elles et al's second result would be much larger than our value if it is extended to 330 nm. In order to better compare our results to others, in the future the same experiments can be performed at a pump wavelength of 266 or 299 nm.

Previously, when we conservatively used an estimated relative yield ratio of "hot" $^{\bullet}OH$ radicals and the prehydrated electrons as r = 2:1 under 330 nm irradiation, we obtained that the prehydrated electron is at least twice as effective as the "hot" OH radicals at causing DNA damage [24]. If we use this r = [$^{\bullet}OH_{hot}$]/$e_{pre}^- = 2.8 \pm 0.4$ value to compare the efficiency of reductive DNA damage induced by the e_{pre}^- with oxidative DNA damage caused by $^{\bullet}OH$, *we will find that* e_{pre}^- *is much more effective at inducing DNA single-strand breaks (SSB) and double-strand breaks (DSB). In terms of SSB and DSB yields per radical,* e_{pre}^- *is nearly 3 times as effective as the "hot" OH radicals at causing DNA damage.* Therefore, the reductive damage of DNA mediated by the e_{pre}^- is a more important pathway in radiotherapy. Hence, this conclusion further proves that understanding the action of the e_{pre}^- is the key to the more efficient radiotherapy.

Moreover, from our observations, we confirmed the existence of a "hot" OH radical state on the ultrafast time scale, analogous to the prehydrated state of the hydrated electron [24]. As it was well known that the OH radicals and prehydrated electrons are co-produced within

1 ps under water radiolysis [20,158], the newly generated OH radical is likely to be in an electronically excited state. Besides the ground state of the OH radical, there are four other electronically excited states of OH radicals in gas-phase[159]. One of those electronic states is a Rydberg state, which has been observed previously in gas-phase studies of OH radicals produced from discharging a condenser through a mixture of O_2, H_2 and He [160]. The "hot" OH radical state proposed in our project is likely to be one of these electronically excited states. However, the details about "hot" OH radical states generated in liquid water under irradiation are not clear. They remain to be elucidated using advanced scientific tools that can detect chemical dynamics on the ultrafast time scale, such as our state-of-the-art fs-TRLS technique.

5.6 Concluding Remarks

This chapter presents the studies of the scavenging reactions between OH radicals and an OH scavenger potassium thiocyanate (KSCN). By detecting the absorption of the reaction products in real time using fs-TRLS, we observed two states of the OH radicals: the hot OH radical state on an ultrafast time scale (~ 1 ps) and the cold state on a much longer time scale (~ a few nanoseconds, corresponding to the previously reported lifetime of OH radicals [11]). The hot OH radical state might be more relevant at inducing biological damage. By comparing the absorption intensities of the reaction product and the hydrated electron, the relative yield ratio of hot OH radicals and the prehydrated electrons r = 2.8 ± 0.4 was obtained. This value proves that the prehydrated electron is nearly twice more effective at inducing DNA damage than the OH radicals.

Chapter 6 Conclusions

Knowledge of the rate constants for the reactions of the prehydrated electron with electron scavengers and OH radical scavengers is needed in order to predict the action of the prehydrated electron in biological events, such as radiotherapy. Moreover, knowing the relative yield ratio r=[OH]/[e_{pre}^-] is necessary to assess the biological effectiveness of OH radicals and the prehydrated electrons at inducing DNA damage under radiotherapy. In this thesis, we present a quantitative study on the rate constants of the prehydrated electron with both electron and OH radical scavengers, as well as a quantitative study on the relative yield ratio of OH radicals and the prehydrated electron using the state-of-the-art femtosecond time-resolved pump-probe laser spectroscopy (fs-TRLS). From our results, we conclude:

- The high reactivity of the prehydrated electron is confirmed from the large reaction rate constant obtained for an electron scavenger, potassium nitrate, with the prehydrated electron. The rate constant $\boldsymbol{k_{pre}}$ = **(0.75 ± 0.5)×10^{13} M^{-1}s^{-1}** is **three orders** larger than the k for the e_{hyd}^- with NO_3^-: $k = 9.7 \times 10^9 \, M^{-1}s^{-1}$.

- From the transient absorption spectra, the decreases in electron yields all take place within 1 ps – giving direct evidence that the scavenging reaction happens between the e_{pre}^- and KNO_3 rather than the e_{hyd}^- and KNO_3.

- One can clearly observe that potassium nitrate with concentration around 2 M can nearly completely quench the prehydrated electron. Therefore, KNO_3 could be used as a good scavenger to assist researchers investigating the electron transfer processes that involve the prehydrated electron.

- The reaction rate constants of the prehydrated electron with isopropanol and DMSO are on the order of magnitude of 10^{11} M^{-1}s^{-1}, which are **two orders** larger than the reaction rate constants of OH radicals with isopropanol and DMSO: $k_{OH} = 2 \times 10^9$ M^{-1}s^{-1} and 7×10^9 M^{-1}s^{-1}, respectively, again confirming the high reactivity of the prehydrated electron.

69

- We present the first direct evidence that ˙OH scavengers isopropanol and DMSO are also effective scavengers of the prehydrated electron using our advanced fs-TRLS technique. When DMSO and isopropanol are applied as OH radical scavengers, their reactions with the prehydrated electron must be taken into account.

- Analogous to the prehydrated and hydrated electron state formed under the radiolysis of water, we observe two different states of OH radicals as well: the "hot" excited OH radical state, with an ultrafast lifetime and the long-lived "cold" OH radical ground states as observed from time-resolved transient absorption spectra.

- Under 330 nm two-phonton UV irradiation, water radiolysis produces "hot" OH radical and the prehydrated electron with a relative yield ratio of 2.8 ± 0.4. Incorporating this ratio into our recent studies on the effectiveness of reductive DNA damage caused by the prehydrated electron, one can conclude that the yield of reductive DNA strand breaks induced by a e_{pre}^- is nearly 3 times as effective as the oxidative DNA strand breaks caused by an OH radical.

In summary, the prehydrated electron generated under water radiolysis is an effective DNA damaging agent in radiotherapy. Understanding the role of the prehydrated electron in radiation-induced reductive DNA damage can shed light on the possible methods that can improve radiotherapy efficiency. The quantitative studies present in our project on the scavenging efficiency of the prehydrated electron by both electron and OH radical scavengers provide important information for regulating the prehydrated electron in biomedical related studies. Moreover, obtaining the quantitative relative yield ratio of the OH radical and the prehydrated electron facilitates the direct comparison of OH radical induced oxidative DNA damage and the prehydrated electron induced reductive damage of DNA.

References

[1] K. Sikora, O. Timbs. Cancer 2025: Introduction, Expert Review of Anticancer Therapy. 4 (2004) S11-S12.

[2] R. H. A. Bradbury P. Cancer, Berlin ;New York : Springer, c2007, 2007.

[3] D. Hanahan, R. Weinberg. The hallmarks of cancer, Cell. 100 (2000) 57-70.

[4] S. B. Brown, E.A. Brown, I. Walker. The present and future role of photodynamic therapy in cancer treatment, The Lancet Oncology. 5 (2004) 497-508.

[5] A. Juarranz, P. Jan, F. Sanz-Rodra-guez, J. Cuevas, S. Gonzalez. Photodynamic therapy of cancer. basic principles and applications, Clinical and Translational Oncology. 10 (2008) 148-154.

[6] C. M. Moore, D. Pendse, M. Emberton. Photodynamic therapy for prostate cancer: a review of current status and future promise, Nat. Clin. Pract. Urol. 6 (2009) 18-30.

[7] M. R. Detty, S.L. Gibson, S.J. Wagner. Current clinical and preclinical photosensitizers for use in photodynamic therapy, J. Med. Chem. 47 (2004) 3897-3915.

[8] A. P. Castano, P. Mroz, M.R. Hamblin. Photodynamic therapy and anti-tumour immunity, Nat Rev Cancer. 6 (2006) 535-545.

[9] N. Somia, I.M. Verma. Gene therapy: Trials and tribulations, Nat. Rev. Genet. 1 (2000) 91-99.

[10] H. Mahroofer, S. Burger, U. Oppitz, M. Flentje, C. Djuzenove. Radiation induced DNA damage and damage repair in human tumor and fibroblast cell lines assessed by histone H2AX phosphorylation, Int. J. Rad. Onco. Biol. Phys. 64 (2005) 573-580.

[11] S. Lehnert. Biomolecular Action of Ionizing Radiation; Taylor & Francis, Boca Raton, 2007.

[12] C.-R. Wang, J. Nguyen, Q.-B. Lu. Bond breaks of nucleotides by dissociative electron transfer of nonequilibrium prehydrated electrons: A new molecular mechanism for reductive DNA damage, J. Am. Chem. Soc. 131 (2009) 11320-11322

[13] P. P. Bera, H. F. Schaefer. (G–H)•–C and G–(C–H)• radicals derived from the guanine·cytosine base pair cause DNA subunit lesions, Proceedings of the National Academy of Sciences of the United States of America. 102 (2005) 6698-6703.

[14] J. F. Ward. DNA damage produced by ionizing radiation in mammalian cells: Identities, mechanisms of formation, and reparability. Prog. Nucleic. Acid. Res. Mol. Biol. 35 (1988) 95-125.

[15] E. J. Alpen. Radiation Biophysics, Academic Press, San Diego, 1998.

[16] B. Albert. Molecular biology of the cell, Garland Science, New York, 2008, pp. 198.

[17] C. Richardson, M. Jasin. Frequent chromosomal translocations induced by DNA double-strand breaks. Nature. 405 (2000) 697-700.

[18] S. Vamvakas, E.H. Vock, W.K. Lutz. On the role of DNA double-strand breaks in toxicity and carcinogenesis. Crit. Rev. Toxicol. 27 (1997) 155-174.

[19] G. V. Buxton, C. L. Greenstock, W. P. Helman, A. B. Ross. Critical review of rate constants for reactions of hydrated electrons, hydrogen atoms and hydroxyl radicals ($^{\bullet}$OH/$^{\bullet}$O^{-}) in aqueous solution, J. Phys. Chem. Ref. Data. 17 (1988) 513-886.

[20] Q.-B. Lu. Effects and applications of ultrashort-lived prehydrated electrons in radiation biology and radiotherapy of cancer. Mutat. Res. 704 (2010) 190-199.

[21] E. J. Hall, A. J. Giaccia. Radiobiology for the Radiologist, Lippincott Williams & Wilkins:, Philadelphia, 2006.

[22] B. D. Michael, P. O'Neill. Molecular biology: A sting in the tail of electron tracks, Science. 287 (2000) 1603-1604.

[23] B. Boudaiffa, P. Cloutier, D. Hunting, M. A. Huels, L. Sanche. Resonant formation of DNA strand breaks by low-energy (3 to 20 eV) electrons. Science. 287 (2000) 1658-1660.

[24] J. Nguyen, Y. Ma, T. Luo, R. G. Bristow, D. A. Jaffray, Q.-B. Lu. Direct observation of ultrafast-electron-transfer reactions unravels high effectiveness of reductive DNA damage, PNAS. 108 (2011) 11783.

[25] H. Abdoul-Carime, L. Sanche. Sequence-specific damage induced by the impact of 3-30 eV electrons on oligonucleotides, Radiat. Res. 156 (2001) 151-157.

[26] G. J. Schulz. Resonances in electron impact on atoms, Rev. Mod. Phys. 45 (1973) 378.

[27] Z. Li, P. Cloutier, L. Sanche, J. R. Wagner. Low-energy electron-induced DNA damage: Effect of base sequence in oligonucleotide trimers, J. Am. Chem. Soc. 132 (2010) 5422-5427.

[28] L. Sanche. Low-energy electron interaction with DNA: Bond dissociation and formation of transient anions, radicals and radical anions, in: M.M. Greenberg (Ed.), Radical and Radical Ion Reactivity in Nucleic Acid Chemistry, John Wiley & Sons, Inc., Hoboken, NJ., 2009, pp. 239-293.

[29] S. W. Botchway, D. L. Stevens, M. A. Hill, T. J. Jenner, P. O'Neill. Induction and rejoining of DNA double-strand breaks in chinese hamster V79-4 cells irradiated with characteristic aluminum K and copper L ultrasoft X rays, Radiat. Res. 148 (1997) 317-324.

[30] P. O. Nikjoo, D. T.Goodhead. Computational modelling of low-energy electron-induced DNA damage by early physical and chemical events, Int. J. Radiat. Biol. 71 (1997) 467-483.

[31] P. Dugal, M. A. Huels, L. Sanche. Low-energy (5-25 eV) electron damage to homo-oligonucleotides, Radiat. Res. 151 (1999) pp. 325-333.

[32] D. Antic, L. Parenteau, M. Lepage, L. Sanche. Low-energy electron damage to condensed-phase deoxyribose analogues investigated by electron stimulated desorption of H- and electron energy loss spectroscopy, The Journal of Physical Chemistry B. 103 (1999) 6611-6619.

[33] H. Abdoul-Carime, P. Cloutier, L. Sanche. Low-energy (5-40 eV) electron-stimulated desorption of anions from physisorbed DNA bases, Radiat. Res. 155 (2001) 625-633.

[34] X. Pan, P. Cloutier, D. Hunting, L. Sanche. Dissociative electron attachment to DNA, Phys. Rev. Lett. 90 (2003) 208102.

[35] L. Sanche. Mechanisms of low energy electron damage to condensed biomolecules and DNA, Radiation Protection Dosimetry. 99 (2002) 57-62.

[36] G. Hanel, B. Gstir, S. Denifl, P. Scheier, M. Probst, B. Farizon, M. Farizon, E. Illenberger, T. Märk. Electron attachment to uracil: Effective destruction at subexcitation energies, Phys. Rev. Lett. 90 (2003) 188104-188107.

[37] H. Abdoul-Carime, S. Gohlke, E. Fischbach, J. Scheike, E. Illenberger. Thymine excision from DNA by subexcitation electrons, Chem. Phys. Lett. 387 (2004) 267-270.

[38] J. Berdys, I. Anusiewicz, P. Skurski, J. Simons. Damage to model DNA fragments from very low-energy (<1 eV) electrons, J. Am. Chem. Soc. 126 (2004) 6441-6447.

[39] J. Berdys, P. Skurski, J. Simons. Damage to model DNA fragments by 0.25-1.0 eV electrons attached to a thymine π^* orbital, The Journal of Physical Chemistry B. 108 (2004) 5800-5805.

[40] F. A. Gianturco, R. R. Lucchese. Radiation damage of biosystems mediated by secondary electrons: Resonant precursors for uracil molecules, J. Chem. Phys. 120 (2004) 7446-7455.

[41] J. Lipfert, J. Llano, L. A. Eriksson. Radiation-induced damage in serine PhosphateInsights into a mechanism for direct DNA strand breakage, The Journal of Physical Chemistry B. 108 (2004) 8036-8042.

[42] X. Li, M. D. Sevilla, L. Sanche. Hydrogen atom loss in pyrimidine DNA bases induced by low-energy electrons: energetics predicted by theory, The Journal of Physical Chemistry B. 108 (2004) 19013-19019.

[43] S. Denifl, S. Ptasińska, G. Hanel, B. Gstir, M. Probst, P. Scheier, T.D. Märk. Electron attachment to gas-phase uracil, J. Chem. Phys. 120 (2004) 6557-6565.

[44] X. Pan, L. Sanche. Mechanism and site of attack for direct damage to DNA by low-energy electrons, Phys. Rev. Lett. 94 (2005) 198104.

[45] K. Aflatooni, A. M. Scheer, P. D. Burrow. Total dissociative electron attachment cross sections for molecular constituents of DNA, J. Chem. Phys. 125 (2006) 054301.

[46] M. Théodore, M. Sobczyk, J. Simons. Cleavage of thymine N_3–H bonds by low-energy electrons attached to base π^* orbitals, Chem. Phys. 329 (2006) 139-147.

[47] S. Tonzani, C. H. Greene. Radiation damage to DNA: Electron scattering from the backbone subunits, J. Chem. Phys. 125 (2006) 094504-7.

[48] S. Tonzani, C. H. Greene. Low-energy electron scattering from DNA and RNA bases: Shape resonances and radiation damage, J. Chem. Phys. 124 (2006) 054312-11.

[49] X. Pan, L. Sanche. Dissociative electron attachment to DNA basic constituents: The phosphate group. Chem. Phys. Lett. 421 (2006) 404-408.

[50] I. Bald, J. Kopyra, E. Illenberger. Selective excision of C_5 from D-ribose in the gas phase by low-energy electrons (0–1 eV): Implications for the mechanism of DNA damage, Angew. Chem. Int. Ed. 45 (2006) 4851-4855.

[51] F. A. Evangelista, H. F. Schaefer. Hydrogen atom and hydride anion addition to adenine: Structures and energetics, Chem. Phys. Chem. 7 (2006) 1471-1480.

[52] D. Huber, M. Beikircher, S. Denifl, F. Zappa, S. Matejcik, A. Bacher, V. Grill, T.D. Märk, P. Scheierc. High resolution dissociative electron attachment to gas phase adenine J. Chem. Phys. 125 (2006) 084303-1.

[53] X. Bao, J. Wang, J. Gu, J. Leszczynski. DNA strand breaks induced by near-zero-electronvolt electron attachment to pyrimidine nucleotides, Proc. Natl. Acad. Sci. 103 (2006) 5658-5663.

[54] J. Gu, Y. Xie, H. F. Schaefer. Near 0 eV electrons attach to nucleotides, J. Am. Chem. Soc. 128 (2006) 1250-1252.

[55] J. Gu, Y. Xie, H. F. Schaefer. Electron attachment to DNA single strands: Gas phase and aqueous solution, Nucleic Acids Res. 35 (2007) 5165-5172.

[56] S. Denifl, P. Sulzer, D. Huber, F. Zappa, M. Probst, T. MÃrk, P. Scheier, N. Injan, J. Limtrakul, R. Abouaf, H. Dunet. Influence of functional groups on the site-selective dissociation of adenine upon low-energy electron attachment, Angewandte Chemie International Edition. 46 (2007) 5238-5241.

[57] A. Kumar, M. D. Sevilla. Low-energy electron attachment to 5'-thymidine monophosphate:â€‰ modeling single strand breaks through dissociative electron attachment, The Journal of Physical Chemistry B. 111 (2007) 5464-5474.

[58] C. Winstead, V. McKoy. Resonant interactions of slow electrons with DNA constituents, Radiat. Phys. Chem. 77 (2008) 1258-1264.

[59] P. Schyman, A. Laaksonen. On the effect of low-energy electron induced DNA strand break in aqueous solution: A theoretical study indicating guanine as a weak link in DNA, J. Am. Chem. Soc. 130 (2008) 12254-12255.

[60] T. Solomun, H. Seitz, H. Sturm. DNA damage by low-energy electron impact: Dependence on guanine content, J. Phys. Chem. B. 113 (2009) 11557-11559.

[61] J. Gu, J. Wang, J. Leszczynski. Electron attachment-induced DNA single-strand breaks at the pyrimidine sites, Nucleic Acids Res. 38 (2010) 5280-5290.

[62] Y. Wang, S. X. Tian. Shape resonance states of the low-energy electron attachments to DNA base tautomers, Phys. Chem. Chem. Phys. 13 (2011) 6169-6175.

[63] J. Berdys, I. Anusiewicz, P. Skurski, J. Simons. Theoretical study of damage to DNA by 0.2−1.5 eV electrons attached to cytosine, J. Phys. Chem. A. 108 (2004) 2999-3005.

[64] S. Gohlke, H. Abdoul-Carime, E. Illenberger. Dehydrogenation of adenine induced by slow (<3 eV) electrons, Chemical Physics Letters. 380 (2003) 595-599.

[65] S. G. Ray, S. S. Daube, R. Naaman. On the capturing of low-energy electrons by DNA, Proc. Natl. Acad. Sci. 102 (2005) 15-19.

[66] S. Ptasinska, S. Denifl, P. Scheier, T.D. Mark. Inelastic electron interaction (attachment/ionization) with deoxyribose, J. Chem. Phys. 120 (2004) 8505-8511.

[67] C. König, J. Kopyra, I. Bald, E. Illenberger. Dissociative electron attachment to phosphoric acid esters: The direct mechanism for single strand breaks in DNA, Phys. Rev. Lett. 97 (2006) 0118105-1-4.

[68] F. Martin, P. D. Burrow, Z. Cai, P. Cloutier, D. Hunting, L. Sanche. DNA strand breaks induced by 0-4 eV electrons: The role of shape resonances. Phys. Rev. Lett. 93 (2004) 0698101-1-4.

[69] A. Kumar, M. D. Sevilla. Role of excited states in low-energy electron (LEE) induced strand breaks in DNA model systems: Influence of aqueous environment, Chem. Phys. Chem. 10 (2009) 1426-1430.

[70] T. Ito, S. C. Baker, C. D. Stickley, J. G. Peak, M. J. Peak. Dependence of the yield of strand breaks induced by gamma-rays in DNA on the physical conditions of exposure: Water content and temperature, Int. J. Radiat. Biol. 63 (1993) 289-296.

[71] N. J. Tao, S. M. Lindsay, A. Rupprecht. Structure of DNA hydration shells studied by Raman spectroscopy, Biopolymers. 28 (1989) 1019-1030.

[72] H. M. Berman. Hydration of DNA, Curr. Opin. Struct. Biol. 1 (1991) 423-427.

[73] E. Westhof (Ed.). Water and Biological Macromolecules, CRC Press Inc., Boca Raton USA, 1993.

[74] M. Huels, L. Parenteau, L. Sanche. Substrate dependence of electron-stimulated O⁻ yields from dissociative electron attachment to physisorbed O_2, J. Chem. Phys. 100 (1994) 3940.

[75] Q.-B. Lu, L. Sanche. Large enhancement in dissociative electron attachment to HCl adsorbed on H_2O ice via transfer of presolvated electrons, J. Chem. Phys. 115 (2001) 5711-5713.

[76] Q.-B. Lu, L. Sanche. Effects of cosmic rays on atmospheric chlorofluorocarbon dissociation and ozone depletion, Phys. Rev. Lett. 87 (2001) 078501.

[77] Q.-B. Lu, L. Sanche. Enhancements in dissociative electron attachment to CF_4, chlorofluorocarbons and hydrochlorofluorocarbons adsorbed on H_2O ice. The Journal of Chemical Physics. 120 (2004) 2434-2438.

[78] J. L. Dye. Electrons as anions, Science. 301 (2003) 607-608.

[79] C. A. Kraus. Solutions of metals in non-metallic solvents; i. General properties of solutions of metals in liquid ammonia, J. Am. Chem. Soc. 29 (1907) 1557-1571.

[80] C. A. Kraus. Solution of metals in non-metallic solvents; ii.1 on the formation of compounds between metals and ammonia, J. Am. Chem. Soc. 30 (1908) 653-668

[81] E. J. Hart, J. W. Boag. Absorption spectrum of the hydrated electron in water and in aqueous solutions, J. Am. Chem. Soc. 84 (1962) 4090-4095.

[82] M.S. Pschenichnikov, A. Baltuska, D.A. Wiersma. Hydrated-electron population dynamics, Chemical Physics Letters. 389 (2004) 171-172,173,174,175.

[83] I. A. Shkrob. The structure of the hydrated electron. part 1. magnetic resonance of internally trapping water anions: A density functional study, J. Phys. Chem. A. 111 (2007) 5223-5231.

[84] V. D. Lakhno. Dynamical polaron theory of the hydrated electron, Chemical Physics Letters. 437 (2007) 198-202.

[85] R. E. Larsen, W. J. Glover, B. J. Schwartz. Does the hydrated electron occupy a cavity? Science. 329 (2010) 65-69.

[86] K. D. Jordan, M. A. Johnson. Downsizing the hydrated electron's lair, Science. 329 (2010) 42-43.

[87] R. Ludwig, D. Paschek. Cavity model challenged: The hydrated electron is localized in regions of enhanced water density, ChemPhysChem. 12 (2011) 75-77.

[88] L. Turi, D. Borgis. Analytical investigations of an electron-water molecule pseudopotential. II. development of a new pair potential and molecular dynamics simulations, J. Chem. Phys. 117 (2002) 6186-6195.

[89] C. M. deLara, T. J. Jenner, K. M. S. Townsend, S. J. Marsden, P. O'Neill. The effect of dimethyl sulfoxide on the induction of DNA double-strand breaks in V79-4 mammalian cells by alpha particles, Radiat. Res. 144 (1995) pp. 43-49.

[90] K. Y. Lam, J. W. Hunt. Picosecond pulse radiolysis—VI. fast electron reactions in concentrated solutions of scavengers in water and alcohols, International Journal for Radiation Physics and Chemistry. 7 (1975) 317-338.

[91] C. D. Jonah, J. R. Miller, M. S. Matheson. The reaction of the precursor of the hydrated electron with electron scavengers, J. Phys. Chem. 81 (1977) 1618-1622.

[92] G. Dolivo, L. Kevan. Optical absorption spectra of localized electrons generated at 1.6 K in polar matrices: Evidence for presolvated electrons, J. Chem. Phys. 70 (1979) 2599-2604.

[93] A. Migus, Y. Gauduel, J. L. Martin, A. Antonetti. Excess electrons in liquid water: First evidence of a prehydrated state with femotosecond lifetime. Phys. Rev. Lett. 58 (1987) 1559-1562.

[94] F. H. Long, H. Lu, K. B. Eisenthal. Femtosecond studies of the presolvated ELectron: An excited state of the solvated electron? Phys. Rev. Lett. 64 (1990) 1469-1472.

[95] S. M. Pimblott, J. A. LaVerne. On the radiation chemical kinetics of the precursor to the hydrated electron, J. Phys. Chem. A. 102 (1998) 2967-2975.

[96] B. Pastina, J. A. LaVerne. Scavenging of the precursor to the hydrated electron by the selenate ion, The Journal of Physical Chemistry A. 103 (1999) 209-212.

[97] R. Laenen, T. Roth, A. Laubereau. Novel precursors of solvated electrons in water: Evidence for a charge transfer process, Phys. Rev. Lett. 85 (2000) 50-53.

[98] Q.-B. Lu, L. Sanche. Enhanced dissociative electron attachment to CF_2Cl_2 by transfer of electrons in precursors to the solvated state in water and ammonia ice, Physical Review B. 63 (2001) 153403-1-152403-4.

[99] Q.-B. Lu, J. S. Baskin, A.H. Zewail. The presolvated electron in water: Can it be scavenged at long range? J. Phys. Chem. B. 108 (2004) 10509-10514.

[100] J. M. Herbert, L. D. Jacobson. Nature's most squishy ion: The important role of solvent polarization in the description of the hydrated electron, International Reviews in Physical Chemistry. 30 (2011) 1-48.

[101] C.-R. Wang, T. Luo, Q.-B. Lu. On the lifetimes and physical nature of incompletely relaxed electrons in liquid water, Phys. Chem. Chem. Phys. 10 (2008) 4463-4470.

[102] C. Silva, P. K. Walhout, K. Yokoyama, P. F. Barbara. Femtosecond solvation dynamics of the hydrated electron, Phys. Rev. Lett. 80 (1998) 1086.

[103] K. Yokoyama, C. Silva, D. H. Son, P. K. Walhout, P. F. Barbara. Detailed investigation of the femtosecond pump-probe spectroscopy of the hydrated electron, The Journal of Physical Chemistry A. 102 (1998) 6957-6966.

[104] M. Assel, R. Laenen, A. Laubereau. Dynamics of excited solvated electrons in aqueous solution monitored with femtosecond-time and polarization resolution, The Journal of Physical Chemistry A. 102 (1998) 2256-2262.

[105] P. Kambhampati, D. H. Son, T. W. Kee, P. F. Barbara. Solvation dynamics of the hydrated electron depends on its initial degree of electron delocalization€ , The Journal of Physical Chemistry A. 106 (2002) 2374-2378.

[106] Z. Vardeny, J. Tauc. Picosecond coherence coupling in the pump and probe technique, Opt. Commun. 39 (1981) 396-400.

[107] A. J. Elliot, F. C. Sopchyshyn. A pulse radiolysis study of I_2^- and $(SCN)_2^{\bullet-}$ in aqueous solutions over the temperature range 15-90°C, Int J Chem Kinet. 16 (1984) 1247-1256.

[108] M. Lebedev, O. Misochko, T. Dekorsy, N. Georgiev. On the nature of "Coherent artifact", Journal of Experimental and Theoretical Physics. 100 (2005) 272-282.

[109] C. W. Luo, Y. T. Wang, F. W. Chen, H. C. Shih, T. Kobayashi. Eliminate coherence spike in reflection-type pump-probe measurements, Opt. Express. 17 (2009) 11321-11327.

[110] X. Shi, F. H. Long, H. Lu, K. B. Eisenthal. Femtosecond electron solvation kinetics in water, J. Phys. Chem. 100 (1996) 11903-11906.

[111] P. J. Rossky, J. Schnitker. The hydrated electron: Quantum simulation of structure, spectroscopy, and dynamics, J. Phys. Chem. 92 (1988) 4277-4285.

[112] Q.-B. Lu, T. Madey. Giant enhancement of electron-induced dissociation of chlorofluorocarbons coadsorbed with water or ammonia ices: Implications for atmospheric ozone depletion, J. Chem. Phys. 111 (1999) 2861.

[113] Q.-B. Lu, T. E. Madey. Negative-ion enhancements in electron-stimulated desorption of CF2Cl2 coadsorbed with nonpolar and polar gases on ru(0001), Phys. Rev. Lett. 82 (1999) 4122.

[114] Q.-B. Lu. Correlation between cosmic rays and ozone depletion, Physical Review Letter. 102 (2009) 118501.

[115] Q.-B. Lu. Cosmic-ray-driven electron-induced reactions of halogenated molecules adsorbed on ice surfaces: Implications for atomspheric ozone depletion and global climate change, Phys. Rep. 487 (2010) 141-167.

[116] Q.-B. Lu. What is the major culprit for global warming: CFCs or CO_2? J. Cosmol. 8 (2010) 1846-1862.

[117] J. E. Aldrich, K.Y. Lam, P.C. Shragge, J.W. Hunt. Fast electron reactions in concentrated solutions of amino acids and nucleotides, Radiat. Res. 63 (1975) pp. 42-52.

[118] Y. Gauduel, S. Berrod, A. Migus, N. Yamada, A. Antonetti. Femtosecond charge separation in organized assemblies: Free-radical reactions with pyridine nucleotides in micelles, Biochemistry (N. Y.). 27 (1988) 2509-2518.

[119] Q.-B. Lu. Molecular reaction mechanisms of combination treatments of low-dose cisplatin with radiotherapy and photodynamic therapy, J. Med. Chem. 50 (2007) 2601-2604.

[120] Q.-B. Lu, S. Kalantari, C.-R. Wang. Electron transfer reaction mechanism of cisplatin with DNA at the molecular level, Molecular Pharmaceutics. 4 (2007) 624-628.

[121] C.-R. Wang, A. Hu, Q.-B. Lu. Direct observation of the transition state of ultrafast electron transfer reaction of a radiosensitizing drug bromodeoxyuridine, J. Chem. Phys. 124 (2006) 241102-4.

[122] C.-R. Wang, Q.-B. Lu. Real-time observation of a molecular reaction mechanism of aqueous 5-halo-2'-deoxyuridines under UV/Ionizing radiation, Angew. Chem. Int. Ed. 46 (2007) 6316-6320.

[123] C.-R. Wang, Q.-B. Lu. Molecular mechanism of the DNA sequence selectivity of 5-halo-2'-deoxyuridines as potential radiosensitizers, J. Am. Chem. Soc. 132 (2010) 14710-14713.

[124] B. Liu, S. B. Nielsen, P. Hvelplund, H. Zettergren, H. Cederquist, B. Manil, B. A. Huber. Collision-induced dissociation of hydrated adenosine monophosphate nucleotide ions: Protection of the ion in water nanoclusters, Phys. Rev. Lett. 97 (2006) 133401.

[125] C.-R. Wang, K. Drew, T. Luo, M. Lu, Q.-B. Lu. Resonant dissociative electron transfer of the presolvated electron to CCl4 in liquid: Direct observation and lifetime of the CCl$_4$*? transition state, J. Chem. Phys. 128 (2008) 041102.

[126] A. H. Zewail. Femtochemistry: Atomic-scale dynamics of the chemical bond using ultrafast lasers (nobel lecture), Angewandte Chemie International Edition. 39 (2000) 2586-2631.

[127] A. H. Zewail. Laser femtochemistry, Science. 242 (1988) 1645-1653.

[128] T. Luo. Femtosecond time-resolved studies on the reaction pathways for the generation of reactive oxygen species in photodynamic therapy by indocyanine green, (2008) .

[129] W. W. Parson. Pump-probe spectroscopy, photon echoes and vibrational wavepackets, 2007, pp. 391-395.

[130] H. E. Lessing, A. Von Jena. Separation of rotational diffusion and level kinetics in transient absorption spectroscopy, Chemical Physics Letters. 42 (1976) 213-217.

[131] A. Ansari, A. Szabo. Theory of photoselection by intense light pulses. influence of reorientational dynamics and chemical kinetics on absorbance measurements, Biophys. J. 64 (1993) 838-851.

[132] A. Hertwig, H. Hippler, A. Unterreiner. Transient spectra, formation, and geminate recombination of solvated electrons in pure water UV-photolysis: An alternative view, Phys. Chem. Chem. Phys. 1 (1999) 5633-5642.

[133] M. J. Bronskill, R. K. Wolff, J. W. Hunt. Picosecond pulse radiolysis studies. I. the solvated electron in aqueous and alcohol solutions, J. Chem. Phys. 53 (1970) 4201-4210.

[134] R. K. Wolff, M. J. Bronskill, J. W. Hunt. Picosecond pulse radiolysis studies. II. reactions of electrons with concentrated scavengers, J. Chem. Phys. 53 (1970) 4211-4215.

[135] J. E. Aldrich, M. J. Bronskill, R. K. Wolff, J. W. Hunt. Picosecond pulse radiolysis. III. reaction rates and reduction in yields of hydrated electrons, J. Chem. Phys. 55 (1971) 530-539.

[136] R. K. Wolff, M. J. Bronskill, J. E. Aldrich, J. W. Hunt. Picosecond pulse radiolysis. IV. yield of the solvated electron at 30 picoseconds, J. Phys. Chem. 77 (1973) 1350-1355.

[137] R. K. Wolff, J. E. Aldrich, T. L. Penner, J. W. Hunt. Picosecond pulse radiolysis. V. yield of electrons in irradiated aqueous solution with high concentrations of scavenger, J. Phys. Chem. 79 (1975) 210-219.

[138] J. W. Hunt, W. J. Chase. Temperature and solvent dependence of electron scavenging efficiency in polar liquids: Water and alcohols, Can. J. Chem. 55 (1977) 2080-2087.

[139] G. Czapski, E. Peled. Scavenging of e$_{aq}^-$ and on the possible breakdown of smoluchowski's equation at high concentrations of solutes, J. Phys. Chem. 77 (1973) 893-897.

[140] J. R. Miller. Scavenging kinetics of electrons produced by irradiation of organic glasses; experimental evidence for long range tunneling, J. Chem. Phys. 56 (1972) 5173-5183.

[141] J. R. Miller. Reactions of trapped electrons by quantum mechanical tunneling observed by pulse radiolysis of an aqueous glass, J. Phys. Chem. 79 (1975) 1070-1078.

[142] H. A. Schwarz. Some applications of time-dependent rate constant theory to radiation chemistry, J. Chem. Phys. 55 (1971) 3647-3650.

[143] B. Pastina, J. A. LaVerne, S. M. Pimblott. Dependence of molecular hydrogen formation in water on scavengers of the precursor to the hydrated electron, J. Phys. Chem. A. 103 (1999) 5841-5846.

[144] T. W. Kee, D. H. Son, P. Kambhampati, P. F. Barbara. A unified electron transfer model for the different precursors and excited states of the hydrated electron, J. Phys. Chem. A. 105 (2001) 8434-8439.

[145] S. W. Shirley, B. H. Stewart, S. Mirelman. Dimethyl sulfoxide in treatment of inflammatory genitourinary disorders, Urology. 11 (1978) 215-220.

[146] D. E. Pegg. Principles of cryopreservation, Cryopreservation and Freeze-Drying Protocols, 2007, pp. 39-57.

[147] R. Chakrabarti, C.E. Schutt. The enhancement of PCR amplification by low molecular-weight sulfones, Gene. 274 (2001) 293-298.

[148] C. G. Elles, I. A. Shkrob, R. A. Crowell, S. E. Bradforth. Excited state dynamics of liquid water: Insight from the dissociation reaction following two-photon excitation, J. Chem. Phys. 126 (2007) 164503-8.

[149] D. N. Nikogosyan, A. A. Oraevsky, V. I. Rupasov. Two-photon ionization and dissociation of liquid water by powerful laser UV radiation, Chem. Phys. 77 (1983) 131-143.

[150] B. H. Milosavljevic, J. A. LaVerne. Pulse radiolysis of aqueous thiocyanate solution, The Journal of Physical Chemistry A. 109 (2005) 165-168.

[151] G. E. Adams, J. W. Boag, B. D. Michael. Reactions of the hydroxyl radical. part 1.-transient spectra of some inorganic radical-anions, Trans. Faraday Soc. 61 (1965) 1674-1680.

[152] J.H. Baxendale, D.A. Stott. Pulse radiolysis of aqueous CNS^- solutions and the rates of hydroxyl-radical reactions, Chem. Commun. (London). (1967) 699-700.

[153] R.B. Draper, M.A. Fox. Titanium dioxide photooxidation of thiocyanate: $(SCN)_2^{\bullet -}$ studied by diffuse reflectance flash photolysis, J. Phys. Chem. 94 (1990) 4628-4634.

[154] R. Zellner, M. Exner, H. Herrmann. Absolute OH quantum yields in the laser photolysis of nitrate, nitrite and dissolved H_2O_2 at 308 and 351 nm in the temperature range 278–353 K, Journal of Atmospheric Chemistry. 10 (1990) 411-425.

[155] E. Szajdzinska-Pietek, J. Gebicki. Pulse radiolytic investigation of perfluorinated surfactants in aqueous solutions, Research on Chemical Intermediates. 26 (2000) 897-912; 912.

[156] G. L. Hug. Optical spectra of nonmetallic inorganic transient species in aqueous solution, National Bureau of Standards, National Standard Reference Data Series. (1981) 1-159.

[157] D. J. Brenner. Stochastic calculations of the fast decay of the hydrated electron in the presence of scavengers--tests of model consistency, International Journal of Radiation Applications and Instrumentation. Part C. Radiation Physics and Chemistry. 32 (1988) 157-162.

[158] B. C. Garrett, D. A. Dixon, D. M. Camaioni et al. Role of water in electron-initiated processes and radical chemistry: Issues and scientific advances, Chem. Rev. 105 (2005) 355-389.

[159] E. de Beer, M. Koopmans, C. de Lange, Y. Wang, W. Chupka. (2+1) resonance-enhanced multiphoton ionization-photoelectron spectroscopy of the OH radical, J. Chem. Phys. 94 (1991) 7634.

[160] A. E. Douglas. Absorption of OH in the 1200 Å region, Can. J. Phys. 52 (1974) 318-323.